ABSTRACT

High-density Intraoperative Brain Monitoring During Cardiac Surgery

Ha Hong Nguyen, M.S.B.M.E

Advisor: Keith Evan Schubert, Ph.D.

Functional near-infrared spectroscopy (fNIRS) is a prominent technique that allows assessment of functional brain activity by measuring hemodynamic responses. Most existing functional brain imaging methods are only capable of examining cerebral oxygenation at the frontal lobes during cardiac surgery; thus, the majority of brain regions remain unmonitored. In an attempt to intraoperatively monitor broader brain regions and detect early oxygen imbalance, high-density fNIRS channels are utilized in this study. A comprehensive test battery of neuropsychological measures is also used to evaluate the subject's cognitive performances pre- and postoperatively and identify cognitive declines following cardiac surgery. The correlation of fNIRS findings and neurocognitive results is analyzed. Since the results are consistent with previous work, the study indicates the use of fNIRS in detecting potential hypoxia. Future research is necessary to further investigate a larger sample with a systematic approach of physiological interference reduction for fNIRS data.

High-density Intraoperative Brain Monitoring During Cardiac Surgery

by

Ha Hong Nguyen, B.S.

A Thesis

Approved by the Department of Electrical and Computer Engineering

---

Kwang Y. Lee, Ph.D., Chairperson

Submitted to the Graduate Faculty of
Baylor University in Partial Fulfillment of the
Requirements for the Degree
of
Master of Science in Biomedical Engineering

Approved by the Thesis Committee

Keith Evan Schubert, Ph.D., Chairperson

Robert J. Marks II, Ph.D.

Jonathan Rylander, Ph.D.

Daniel Lee, M.D.

Accepted by the Graduate School
May 2019

J. Larry Lyon, Ph.D., Dean

Page bearing signatures is kept on file in the Graduate School.

TABLE OF CONTENTS

LIST OF FIGURES

LIST OF TABLES

ACKNOWLEDGMENTS

I want to express my great appreciation to my advisor, Dr. Keith Schubert for his generous support, valuable guidance, and constructive advises throughout the development of this research work. I would also like to thank Dr. Daniel Lee for enabling me to be a part of in this research and Dr. Jared Benge for providing helpful insight on neurocognitive aspects of the study. Lastly, I wish to express my sincere thanks to my family for their unconditional love and support.

To my Mother, for everything

CHAPTER ONE

Introduction

Despite the advances of surgical technologies, neurological complications following cardiovascular surgery have remained as a major concern in clinical care. These adverse outcomes include a wide range of disorders running from lethal stroke or comma to encephalopathy, delirium, and more common, neurocognitive deficits [11].

Postoperative cognitive dysfunction (POCD) is not well-defined but generally described as a decline in cognitive functions subsequent to cardiac surgery [12]. Some studies have showed that patients with minor cognitive changes can return to their normal functions in daily life within several weeks [13]. On the other hand, the symptoms of patients with POCD tend to last for months, resulting in long-term disability [13]. Patients suffering adverse complications often require intensive care and thus prolongs the hospital stay. As a result, POCD is associated with an increase in medical costs and a decrease in quality of life. In more severe case, it leads to intermediate-term mortality [13, 14].

There are several potential factors of POCD: the effects of anesthesia, the systemic inflammatory responses related to cardiopulmonary bypass (CPB), and cerebral damage [11, 15]. Conceptually, POCD is subtle and can vary depending on particular brain regions. Although there is no well-established diagnostic strategies to determine POCD, the phenomenon can be identified via a series of psychological tests that exploit four main cognitive domains: 1) verbal learning and memory, and language language comprehension; 2) abstraction and visuospatial orientation; 3) attention, psychomotor processing speed, and concentration; 4) visual memory [16]. However, the neurological evaluation can neither localize the areas of brain damage nor define the underlying causes of brain injury.

Brain hypoxia, a common pathway to cerebral damage, is a dangerous condition in which oxygen demand at the tissue level surpasses oxygen supply [17]. Continuous monitoring of cerebral oxygenation allows detection of early oxygen imbalance and potentially decreases the probability of adverse events [17]. Among functional neuroimaging techniques such as electroencephalography (EEG) and functional magnetic resonance imaging (fMRI), the most promising continuous intraoperative neuromonitoring method is functional near-infrared spectroscopy (fNIRS) [18].

1.1 Current State of Technologies

Functional brain imaging technologies have provided more in-depth insights of the brain to human discovery and hence became viable tools in many studies of brain-related conditions, especially those related to POCD occuring after cardiac surgery [19]. Data acquired from imaging modalities have temporal and spatial resolution. Temporal resolution refers to the precision of the measured activity corresponding to the timing of the actual neuronal activity, while spatial resolution refers to the accuracy of the measured activity corresponding to the location within the brain [19]. Functional brain imaging modalities access brain activity in the localized areas through direct and indirect imaging methods.

The direct imaging techniques include electroencephalography (EEG) and magnetoencephalography (MEG). EEG captures the electrical activity generated by neural firing, whereas MEG detects the magnetic fields generated by neural electrical activity [20]. These two techniques produce excellent temporal resolution; however, the spatial information provided by EEG is very low and the overall system of MEG is highly sensitive to motion artifacts [20, 21].

In contrast, positron emission tomography (PET) and functional magnetic resonance imaging (fMRI) are indirect imaging techniques that rely on the hemodynamic changes rather than electrical signals [19]. Hemodynamic changes are defined as changes in blood flow due to an increase in energy demands during brain activity.

PET measures blood flow, using radioactively labeled molecules, called tracers that are introduced to the body through injection or inhalation [21]. Similar to PET, fMRI creates a map of brain activation and detects increased blood flow at the greater active brain regions. PET and fMRI have high spatial and low temporal resolution [19]. The operating system of PET and fMRI requires heavy, bulky, and expensive machinery with additional costs of labor and intense machine training, hindering the use of imaging modalities across clinical settings [21].

1.2 Functional Near-infrared Spectroscopy (fNIRS)

William Herschel discovered near-infrared light in the 1800's; however, the feasibility of near-infrared spectroscopy (NIRS) in monitoring cerebral oxygenation of brain tissue was first examined by Frans Jobsis in 1977 [22]. In 1980s, Marco Ferrari utilized NIRS intrsuments to study cerebral oxygenation in experimental animals and human adults [5]. As the technique was advancing, four different research groups in 1993 successfully demonstrated the use of NIRS in investigating human brain functions by monitoring changes in prefrontal cortex oxygenation [22]. In 1994, the first clinical application of NIRS in psychiatry was presented in Okada's study of patients affected by chronic schizophrenia [5]. For the purpose of functional brain studies, the technique was then named as functional near-infrared spectroscopy (fNIRS) [22].

Functional near-infrared spectroscopy (fNIRS) is an optical and indirect imaging modality that utilizes the low levels of light in the near-infrared (NIR) spectrum (Figure 3.1) to non-invasively measure the cerebral hemodynamic changes, resulting from brain activation at the regions of interest over time [22]. The fNIRS operating system consists of two main components: a light source that emits two or more wavelengths in the NIR window, and a detector that measures light intensity after transmission through the sample. Since the NIR light can penetrate up to 2 cm deep into the adult head, the technique measures the cortical surface activity of

the brain [23]. The modified Beer-Lambert law (Equation 3.2) is the most common algorithm that quantifies the amount of light attenuation, which is proportional to the changes in concentrations of oxygenated [HbO_2] and deoxygenated [Hb] hemoglobin. The relative changes in hemodynamic response can be used as an indirect measure of cerebral oxygenation, providing an insight into brain activation [8].

In comparison to PET and fMRI, fNIRS provides higher temporal resolution; however, due to its limited depth penetration, fNIRS fails to sample the deep-brain regions below the cortical surface, resulting in low spatial resolution [24]. Regardless, fNIRS has significant advantages that overcome shortcomings of other traditional imaging modalities. fNIRS measurements can be taken continuously and repeatedly due to the use of low-energy NIR light. Furthermore, the fNIRS system is highly resistant to motion artifacts, making it suitable for imaging infants, children, and subjects with movement disorders, like Parkinson's diseases [24]. The equipment is relatively low-cost, compact, portable and therefore allows a variety of testing locations with high environmental constraints [22, 24]. Given these characteristics, the fNIRS technique is ideal for studying functional brain activity in the operating room (OR) during cardiac surgery.

fNIRS technology, as reviewed by Quaresima et.al, has become a popular imaging tool used in various research fields, including brain physiology and disease progression, behavioral and cognitive developments in adults, psychiatry, stroke, and brain injury [24]. In addition to its popularity among researchers, fNIRS has been increasingly applied as a real time brain-monitoring device to detect blood oxygenation during cardiac surgery [17, 25]. Several commercially available fNIRS-based cerebral oximeters are INVOS, FORE-SIGHT, and EQUANOX. These current technologies are only capable of monitoring cerebral oxygenation at the frontal lobes of the brain due to the limited area of application and the nature of the device's design (Figure 1.1a) [1, 26–28]. As a result, the information about cerebral oxygenation

within other regions of the brain remain unmonitored. Damage at these brain regions, however, may pose a high risk of POCD.

The study proposes the utility of high-density fNIRS channels as an intra-operative monitoring modality. As shown in Figure 1.1b, the technique monitors broader brain regions, including prefrontal cortex, frontal lobes, and posterior parietal cortex. Detection of potential hypoxic events is implemented in off-line data analysis. Further, the correlation between fNIRS findings and neurological evaluations is also investigated.

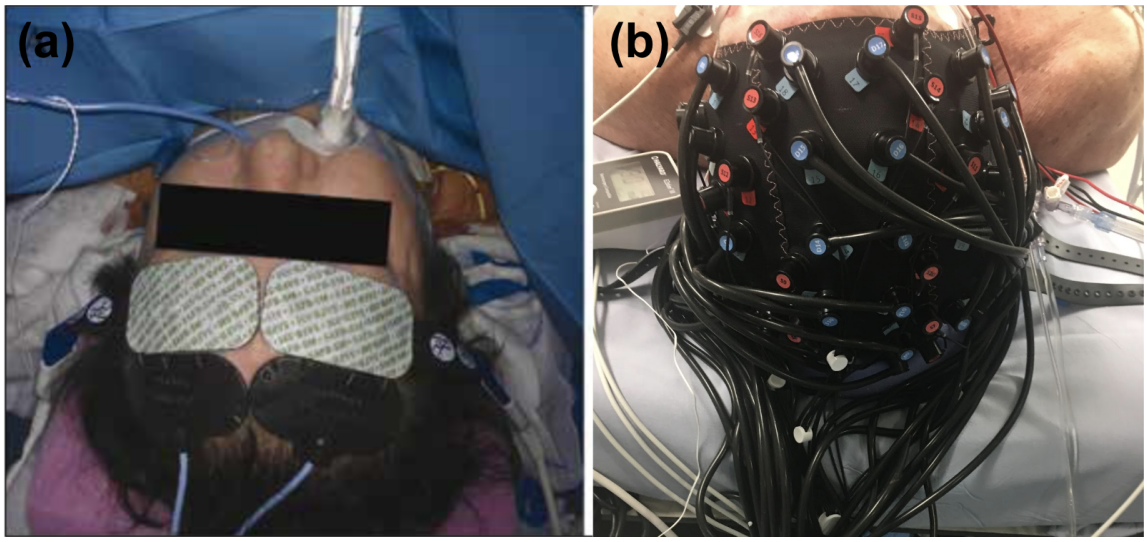

Figure 1.1. (a) Common cerebral oximeters: INVOS and EQUANOX [1], (b) high-density fNIRS system used in this study.

1.3 Thesis Outline

The following list outlines the remaining chapters of the study.

Chapter Two

Background explains biological basis of hemoglobin, oxygenation, brain anatomy, and optical properties of tissues and provides an overview of coronary artery bypass grafting (CABG).

Chapter Three

Literature Review discusses general principles of fNIRS and neurocognitive measures which are often used to identify cognitive impairments.

Chapter Four

Instrumentation presents basic components of fNIRS imaging technique and reviews experimental instrument used in the study.

Chapter Five

Methodology describes the experimental design of the study, consisting of fNIRS imaging technique and neurocognitive assessments.

Chapter Six

Results and Discussion report two case studies through the individual's neurocognitive evaluations and fNIRS findings.

Chapter Seven

Conclusion provides a summary of the study, research limitations, and directions for future work.

CHAPTER TWO

Background

2.1 Hemoglobin

Hemoglobin is a protein in red blood cells which carries oxygen throughout the body. It consists of two pairs of polypeptide chains, called globin chains [29]. Each globin chain surrounds a heme group that has an iron atom at its center to which oxygen binds. Therefore, each hemoglobin can carry up to four oxygen molecules, forming oxygenated hemoglobin [HbO_2] [29]. Similarly, deoxygenated hemoglobin [Hb] is formed upon the release of bounded oxygen.

2.2 Blood Oxygenation

The heart plays an essential role in blood circulation while the lungs control blood oxygenation. The deoxygenated blood from the body travels to the right chambers of the heart and is pumped through a pulmonary artery to the lungs where it exchanges oxygen [O_2] and removes carbon dioxide [CO_2]. The oxygenated blood then returns from the lungs back into the left chambers of the heart and is pumped to the brain and the rest of the body. The heart and lungs work closely together to supply nutrients and transport oxygen to targeted organs, allowing them to function properly.

Mixed venous oxygen saturation [SvO_2] is a percent of the remaining oxygen measured at the pulmonary artery after tissue oxygen consumption. Its normal range for a healthy individual is from 65-80% [30]. A decrease in [SvO_2] implicates an insufficiency in oxygen supply or an increase in oxygen consumption [30]. These conditions potentially lead to hypoxia, causing irreversible tissue damage after a long duration. In previous studies, different threshold values of [SvO_2] have been utilized to identify hypoxia in patients undergoing cardiac surgery. Results from Holm's study

have found that patients with $[SvO_2]$ below 60% have longer hospital stay, higher 30-day mortality after surgery, and lower 5-year survival rate [31]. On the other hand, Krauss's study used a threshold of 65% of $[SvO_2]$ to indicate postoperative complications [32]. Even though there is no well-established cut-off for $[SvO_2]$, the parameter is an useful indicator of potential hypoxia.

2.3 Coronary Artery Bypass Graft (CABG)

Coronary artery bypass grafting (CABG) is an open-heart procedure in which a healthy blood vessel, an artery or vein taken from the patient's chest, leg or arm, is grafted from the aorta to the blocked coronary artery [33]. As presented in Figure 2.1, the grafted blood vessel bypasses the blockage portion of the coronary artery and creates a new path for blood to flow to the heart. CABG is an invasive surgery because the surgeon opens the patient's chest cavity, exposes the heart, and repairs it. During a surgical duration, the patient's core temperature is lowered to a state of moderate hypothermia, ranging from 27 to 32 degrees Celsius [34].

2.3.1 Cardiopulmonary Bypass (CPB)

Generally, operating on the beating heart is very challenging because of the heart motion and the blood flow inside the heart. As a result, the heart must be temporarily stopped from beating and directly connected to the cardiopulmonary bypass (CPB) device, also known as the heart-lung machine, that mimics the functions of heart and lung [35]. The heart-lung machine allows blood to completely bypass the heart and lungs while it mechanically maintains the circulation of blood and automatically regulates oxygen levels of the body. As illustrated in Figure 2.2, the CPB system consists of five main components: reservoir, pump, heat exchanger, oxygenator, and arterial filter [36]. The deoxygenated blood is passively drained via venous cannula from the large veins into the reservoir of the machine. The suctioned blood is driven via the pump into the heart exchanger, which is used to cool the blood

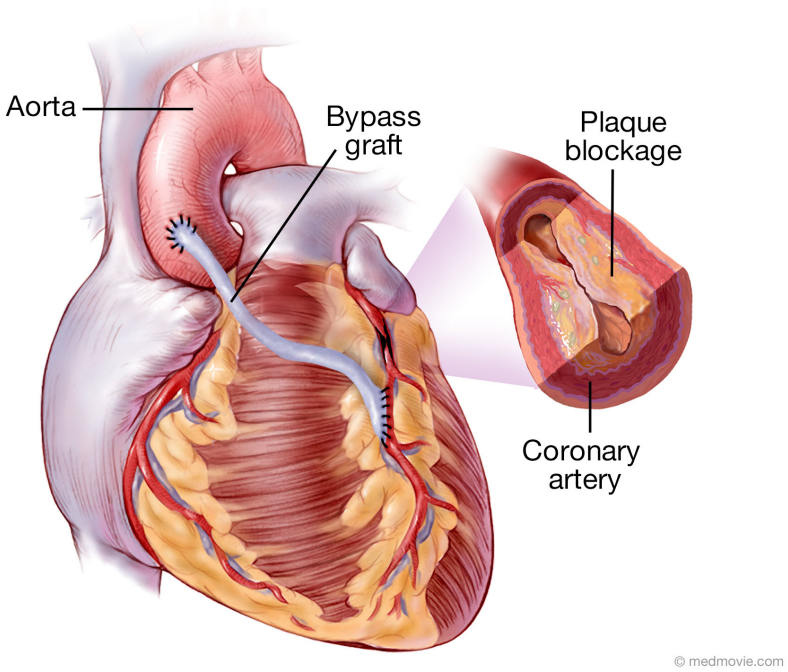

Figure 2.1. An overview of Coronary Artery Bypass Grafting (CABG), an invasive surgery that restores blood flow by grafting a healthy blood vessel to bypass the blocked coronary artery [2]

during the cardiac repair and rewarm the blood during the weaning of CPB. The blood flows from the heat exchange system to the oxygenator or artificial lung, where it absorbs oxygen [O_2] and discards carbon dioxide [CO_2] [35, 36]. Before returning to the patient's body, the oxygenated blood must pass through an arterial filter that is made of micro-porous materials to reduce debris, fibrin, and air bubbles [3]. These matters can be accidentally introduced into the blood circulation during CPB duration, cause embolisms, and pose a high risk of brain injury. Finally, the CPB machine pumps the filtered blood back to the body through the arterial cannula.

2.3.2 Cardioplegia System

During an open-heart surgery, the heart is drained of blood by the CPB machine, and a cross clamp placed on the ascending aorta is used to isolate the heart from the rest of blood circulation [36]. These steps allow a bloodless, motionless, and operative field; however, the procedure completely interrupts oxygen and nutrient

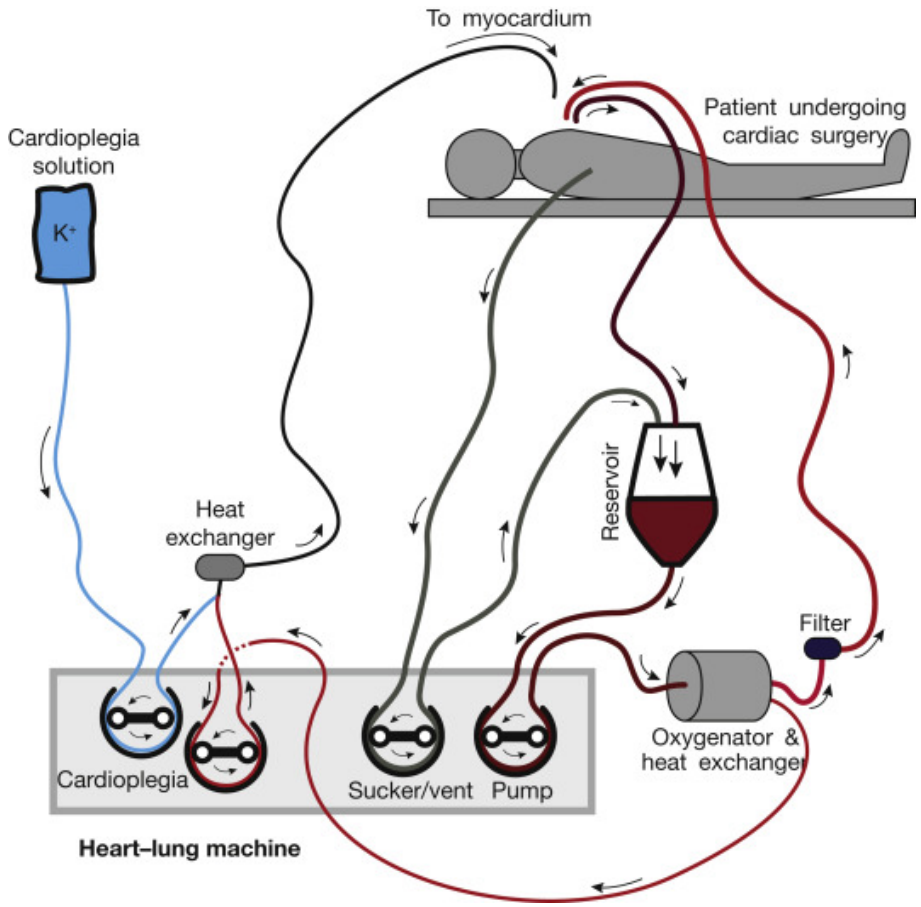

Figure 2.2. A diagram of cardiopulmonary bypass during cardiac surgery. The deoxygenated blood is completely drained into reservior and generated with oxygen in oxygenator. The oxygenated blood passes through a filter and returns back to the heart; meanwhile, a portion of the blood is mixed with cardioplegic solution for myocardial protection and also returns back to the heart [3]

supply to the heart. The low levels of oxygen are not enough to meet myocardial metabolism, leading to cell death and eventually heart ischemic [3]. Protecting the heart against ischemia is often required to increase ischemic tolerance of the heart, as well as preserving myocardial functions. Cardioplegia is a technique of myocardial protections in which the heart is perfused with cardioplegic solution to halt electrical pulses and contractions of the heart and therefore lower the metabolic rate of the myocardium and prevent cell death [36]. In Figure 2.2, after being generated with oxygen, a portion of the blood is mixed with chemical agents and returns to the heart to preserve myocardium.

2.4 Brain Anatomy

The human brain is the most important and complex feature in charge of all body functions, ranging from forming thoughts to producing actions. The brain is enclosed and protected by a hard bony shell, called the skull [37]. Underneath the skull is cerebrospinal fluid which is a clear, colorless liquid that surrounds the brain and serves as shock absorber [37]. As presented in Figure 2.3, the cerebrum, cerebellum. and brainstem are three main components of the brain.

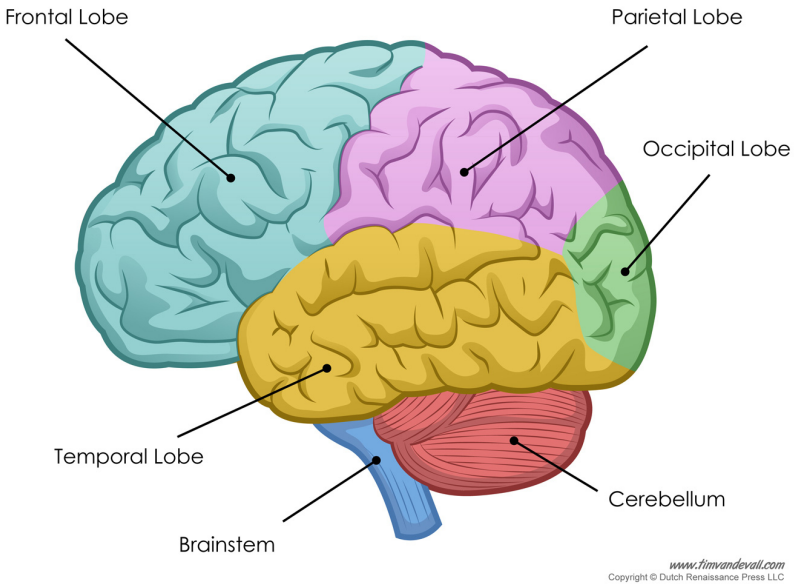

Figure 2.3. Brain anatomy: cerebrum, cerebellum, and brain stem. Cerebrum is divided into four regions: frontal, parietal, temporal, and occipital lobes [4]

Cerebrum is the largest part of the brain and plays a key role in language, thoughts, sensors, and movements. The cerebrum consists of two halves: the right and left hemispheres which are connected by a bundle of fibers [37]. Each hemisphere controls the opposite side of the body. While the right hemisphere is dominant for visual-spatial abilities, the left hemisphere is more dominant for language and logic abilities [37].

The outermost layer of cerebrum is the cerebral cortex, where most information processing occurs. The cerebral cortex is divided into four sections: frontal, parietal,

temporal, and occipital lobe, and each lobe controls different functions [37]. The frontal lobe is in the front of the brain and is responsible for motions, emotions, and higher level of cognition, for instance, thinking, language, and problem solving [38]. The parietal lobe is behind the frontal lobe and is associated with processing visuospatial orientation and interpreting sensory information, such as touch and pain. The occipital lobe is at the back of the brain and is a major processing center of visual information [38]. The temporal lobe is at the bottom of the brain and is involved in memory and auditory processing. Finally, cerebellum is responsible for coordination, posture, and balance while brain stem controls automatic functions, for example, heart rate, blood pressure, and respiration [37].

2.5 Neurovascular Coupling

Neurons are nerve cells that make up the majority of the human brain. The basic function of neurons is to receive and send information to one another through electrical and chemical signals. The brain activity leads to neural activation which is correlated to the subsequent changes in cerebral blood flow (CBF), cerebral blood volume (CBV), and blood oxygenation [39]. When neurons activate within a localized brain region, there is a significant increase in oxygen metabolism. An increase in oxygen consumption leads to a decrease in tissue oxygenation [39]. Blood vessels dilate to allow more blood flow to the active region, compensating for high oxygen demand.

The relationship between local neural activity and CBF regulation is defined as neurovascular coupling. During this coupling, the body tends to overcompensate the needs of energy [40]. As a result, the amount of oxygen supplied is often greater than that consumed. This leads to a significant rise of oxygenated hemoglobin [HbO_2] and a slight decrease of deoxygenated hemoglobin [Hb] at the active region (Figure 2.4). Consequently, the total hemoglobin or a sum of [HbO_2] and [Hb] increases [5, 40]. The changes in concentrations of oxygenated and deoxygenated hemoglobin closely

correspond to the changes in regional CBF and CBV that are caused by neural activation. The hemodynamic response, therefore, is an indirect measure of brain activity [39].

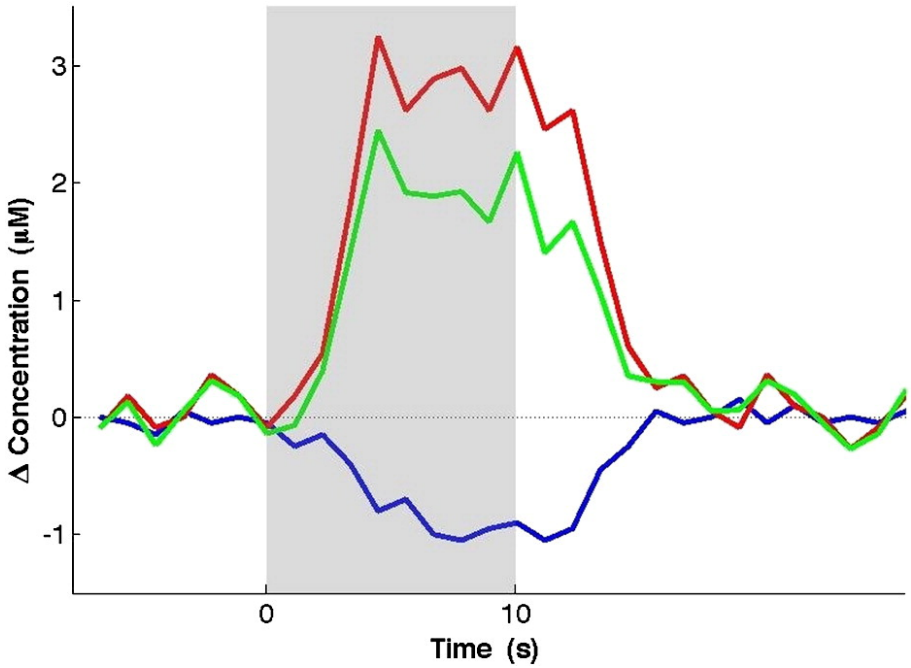

Figure 2.4. A typical hemodynamic response curve. During neural activation (gray shadow), oxygenated hemoglobin [HbO_2] (red line) increases, and deoxygenated hemoglobin [Hb] (blue line) decreases. This results in an increase of the total hemoglobin (green line) [5]

2.6 Optical Properties of Tissues

When light penetrates into biological tissues, scattering and absorption are the two main light-tissue interactions dependent on the wavelengths of light and the optical properties of tissues. The optical properties such as refractive index and corresponding angle of incidence are determined by constituent components of tissues and propagation of light [41].

Optical scattering occurs when photons change direction of propagation due to the refractive index mismatch between the tissue and its surrounding medium. Approximately 80% of light attenuation, or intensity loss, is caused by scattering,

and the remaining 20% by absorption [6]. Multiple scattering increases the distance photons travel and leads to a higher probability of photons being absorbed in tissues [6]. The absorption process happens when the energy of a photon is transferred to a chromophore, a part of a molecule that absorbs light. The common chromophores in tissues are water, lipids, melanin, and hemoglobin [41]. Each chromophore has a different absorption spectral and thus can be identified by using different wavelengths.

For non-scattering media, the Beer-Lambert law (BLL), described in Equation 2.2, is a linear model that correlates the absorbance to the concentration of a given chromophore and the distance travelled by light [6].

$$A = -\log(\frac{I}{Io}) \tag{2.1}$$

$$= \varepsilon * C * L \tag{2.2}$$

where A is the absorbance (or light attenuation), Io is the incident light intensity, I is the transmitted intensity through medium, ε is the molar extinction coefficient, C is the concentration of a particular chromophore, and L is the optical path length that light travels through medium.

CHAPTER THREE

Literature Review

This chapter provides general knowledge of fNIRS technique (Section 3.1) and discusses neurocognitive aspects of the study (Section 3.2).

3.1 Functional Near-infrared Spectroscopy (fNIRS)

3.1.1 Principles of fNIRS

Biological tissues are relatively transparent in the near-infrared spectrum, which is also referred to as an optical window that ranges from 650-960 nm (Figure 3.1). Even though water is the main component of tissues, it absorbs very little light within the NIR region. In addition, other substances such as melanin and collagen have higher absorption coefficients, but their concentrations are relatively low [42]. In consequence, oxygenerated [HbO_2] and deoxygenated [Hb] hemoglobin are two dominant tissue chromophores in the optical window.

When studying brain functions, the light sources are often coupled against patient's head to irradiate NIR wavelengths, and the detectors are placed just a few centimeters away from sources to collect the returning photons. Due to the systemic configuration and scattering effects of tissues, photons travel in a banana-shaped path rather than follow a linear distance between the source and the detector (Figure 3.2) [7]. This results in an increased optical path length travelled by photons and hence leads to a higher probability of light absorption in tissues. For adults' head, NIR light can typically sample a diffuse volume that is roughly 2 cm below the human skin [23]. Before reaching the grey matter (0.5 - 1 cm), NIR light passes through the superficial layers, including the scalp (0.5-1 cm), the skull (0.5-1 cm), and the cerebral spinal fluid (0.2 mm) [43]. The thickness of these layers varies depending on age,

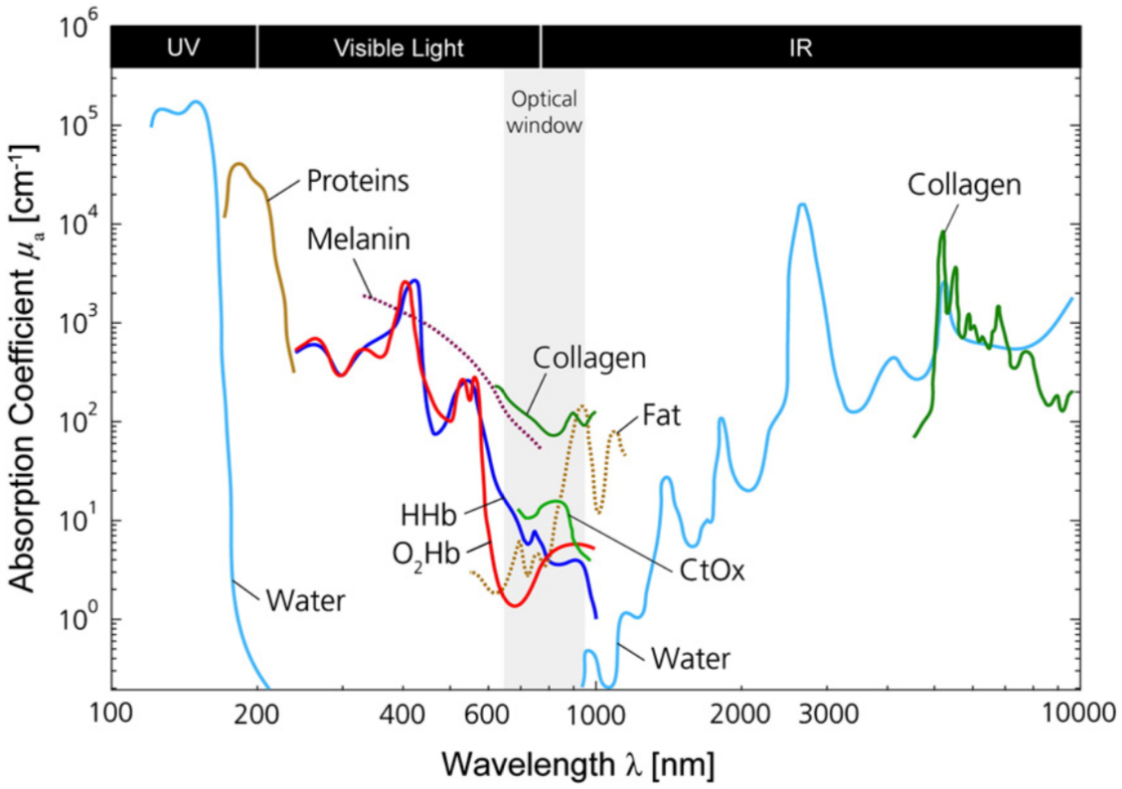

Figure 3.1. Absorption spectra of HbO_2 and Hb within optical window [6]

gender, and inter-subject factors. Therefore, it results in differences of depth sampling between individuals and also affects the spatially sensitivity of fNIRS measurements.

The penetration depth is a measure of how far light can penetrate into tissue at a given wavelength. It is determined as one third to one half of the source-detector (SD) separation distance [23]. In general, the greater the SD distance, the deeper the light penetration. However, the light intensity captured by a detector decreases as the SD distance increases [23]. There must be a limit of separation distance to obtain meaningful fNIRS measurements. Previous studies have examined the depth penetration at various SD distances. Naseer's study has showed that a separation distance less than 1 cm may only sample the superficial layers of the head, whereas SD distance more than 5 cm may result in weak and unstable signals [7]. The reported results from Strangman's study have suggested that the ideal SD separation for the adult brain should be around 3-3.5 cm to ensure sensitivity to brain tissues while

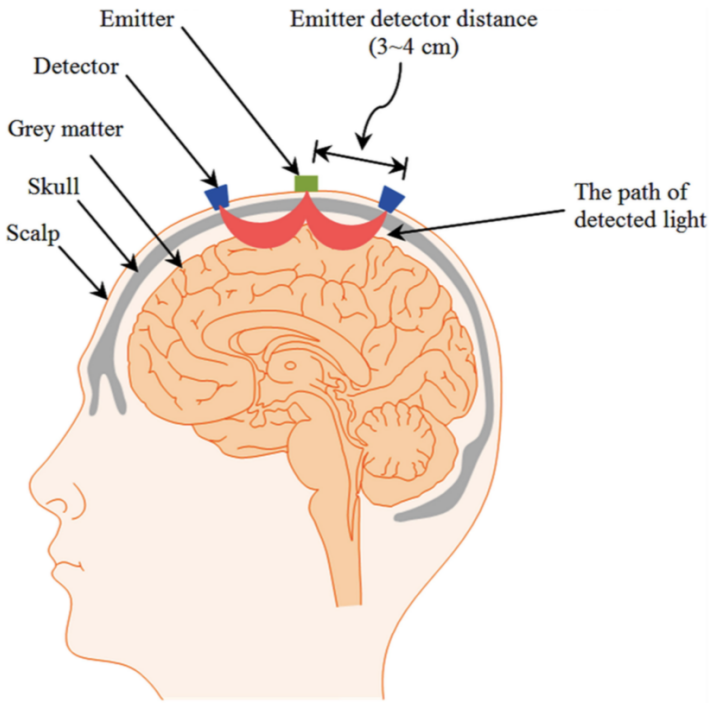

Figure 3.2. A typical setup of a source and a detector results in the banana path-length of NIR light [7]

achieving an adequate depth penetration of 1.5-2 cm [44]. Several factors that affect the selection of optimal SD distance include NIR light intensity, wavelength, head regions, age and gender of the subject [44].

3.1.2 Optical Imaging Theory

The simple BLL is not applicable for quantification of chromophores in highly scattering medium such as biological tissues. A modified Beer-Lambert law (MBLL) was developed to account for the increased distance travelled by light due to multiple scattering in tissues [43]. In addition, partial volume corrections must also be considered in the MBLL to account for the absorption over a small fraction of the sampling volume [43]. The total absorption is measured in optical density (OD) and expressed

by the Equation 3.2

$$OD = -\log(\frac{I}{Io}) \tag{3.1}$$

$$= \varepsilon * C * L * B + G \tag{3.2}$$

where B is a scaling factor, also known as a differential pathlength factor (DPF), and G is a geometry parameter which accounts for an amount of light loss, due to scattering, before light reaching detector. The DPF is a correction term used to adjust the increased optical path length and the partial volume factor in the scattering medium. Numerous studies have been conducted to determine the DPF approximation for different tissues types, wavelengths, and inter-subject variation [43]. In most functional brain studies, it is more important to detect relative changes of absorption varying in time than to quantify total absorption in absolute values. According to the MBLL, a change in the chromophore concentration is proportional to a change in the light intensity detected [23]. With the assumption that B and G remain constant, the total changes in optical density is shown in Equation 3.3

$$\Delta OD^{\lambda} = \varepsilon^{\lambda} * \Delta C * L * B^{\lambda} \tag{3.3}$$

where λ is a specific wavelength. As previously stated, oxygenated $[HbO_2]$ and deoxygenated [Hb] hemoglobin are main light absorbers in the NIR spectrum. Each form of hemoglobin has a distinct absorption spectra, and an isosbestic point, where $[HbO_2]$ and [Hb] have the same absorption coefficient, is near 810 nm [27]. Typically, at least two wavelengths are needed to determine the concentration of chromophores [23]. The measurement of $[HbO_2]$ is sensitive to a wavelength above the isosbestic point, while that of [Hb] is sensitive a wavelength below the isosbestic point [42]. The linear relationship between the change in optical density and the change in concentration of each chromophore present in the sample is defined in the following

expression

$$\Delta OD^{\lambda_1} = (\varepsilon^{\lambda_1}_{HbO_2} * \Delta HbO_2 + \varepsilon^{\lambda_1}_{Hb} * \Delta Hb) * L * B^{\lambda_1} \tag{3.4}$$

$$\Delta OD^{\lambda_2} = (\varepsilon^{\lambda_2}_{HbO_2} * \Delta HbO_2 + \varepsilon^{\lambda_2}_{Hb} * \Delta Hb) * L * B^{\lambda_2} \tag{3.5}$$

From Equation 3.4 and Equation 3.5, the concentration changes of $[HbO_2]$ and [Hb] can be calculated by Equation 3.6 and Equation 3.7 repectively

$$\Delta HbO_2 = \frac{(\varepsilon^{\lambda_1}_{Hb} * \Delta OD^{\lambda_2})/B^{\lambda_2} - (\varepsilon^{\lambda_2}_{Hb} * \Delta OD^{\lambda_1})/B^{\lambda_1}}{(\varepsilon^{\lambda_2}_{HbO_2} * \varepsilon^{\lambda_1}_{Hb} - \varepsilon^{\lambda_1}_{HbO_2} * \varepsilon^{\lambda_2}_{Hb}) * L} \tag{3.6}$$

$$\Delta Hb = \frac{(\varepsilon^{\lambda_1}_{HbO_2} * \Delta OD^{\lambda_2})/B^{\lambda_2} - (\varepsilon^{\lambda_2}_{HbO_2} * \Delta OD^{\lambda_1})/B^{\lambda_1}}{(\varepsilon^{\lambda_1}_{HbO_2} * \varepsilon^{\lambda_2}_{Hb} - \varepsilon^{\lambda_2}_{HbO_2} * \varepsilon^{\lambda_1}_{Hb}) * L} \tag{3.7}$$

3.1.3 Types of fNIRS Systems

The fNIRS implementations are categorized based on the principles of how the light is transmitted through human tissues. Three types of fNIRS techniques are continuous waves (CW), frequency domain (FD), and time domain (TD) (Figure 3.3). Compared to CW systems, light in TD and FD systems penetrates deeper into tissue and therefore yields better sensitivity to cerebral hemodynamic features [45].

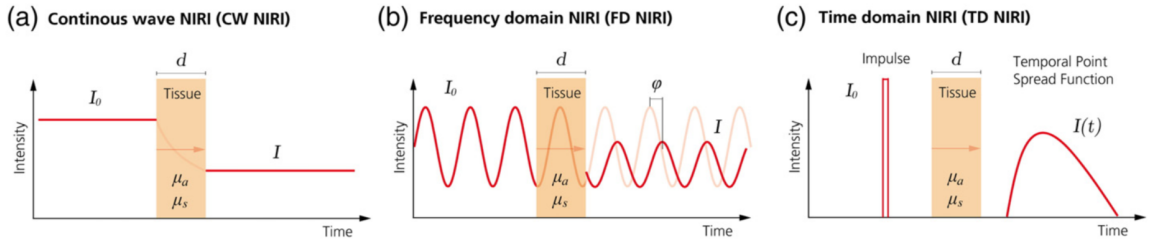

Figure 3.3. Three main types of fNIRS systems [8]

In TD systems, the light is delivered in extremely short pulses (picosecond). These pulses are broadened because photons, when traversing biological tissues, are scattered in different directions [45]. This property enables the TD system to detect

the distribution of time-of-fight, an amount of time the light travels through tissues. By using the time-of-flight of photons and the speed of light, the optical traveling pathlength can be directly measured [23]. Therefore, TD systems allow quantification of $[HbO_2]$ and [Hb] hemoglobin concentrations in absolute terms. Even though TD methods can obtain the highest spatial resolution, it requires a long acquisition time to achieve a reasonable signal-to-noise ratio (SNR), a measure of signal strength relative to background noise, and thus results in a relatively low temporal resolution.

FD systems modulate the emitted light intensity at frequencies of 10-100MHz. The attenuated intensity and phase shift of the transmitted light provide a direct measure of absorption and scattering coefficients [8]. FD methods are capable of quantifying the absolute $[HbO_2]$ and [Hb] concentrations. The temporal resolution of FD signals is higher than that of TD signals, but is lower than that of CW signals [45]. In general, instrumentation used in either TD or FD systems is high cost and complex.

CW systems continuously illuminate tissues at constant light intensity. In contrast to FD and TD methods, only the detected light intensity is measured in CW methods [45]. Therefore, CW systems cannot determine the absolute values of $[HbO_2]$ and [Hb] concentrations. Instead, with estimations of path length photon travelled, the relative changes can be calculated via the MBLL. Compared to the TD and FD imaging modalities, CW systems obtain the best SNR at the sampling frequency above 1 Hz [23]. Although TD and FD systems provide more hemodynamic information in deeper-brain regions, these two techniques are more expensive and less accessible than the CW methods. Due to its low cost, simplicity, and portability, the CW-fNIRS system has widely extended its applications in brain studies and clinical practices.

3.2 Neurocognitive Measures

As outlined in the 1995 Statement of consensus on assessment of neurobehavioral outcomes after cardiac surgery, a test battery consisting of six neuropsychological tests (Appendix A) is selected for this study [46]. As shown in Table 3.1, each neurocognitive test is associated with particular cognitive domains. Pre- and postoperative assessments in patients undergoing cardiac surgery are required to determine whether patient's cognitive performance is declined [47].

Table 3.1. Neurocognitive Measures and Corresponding Cognitive Domains

Measure	Abbreviation	Cognitive Domain
Rey Auditory Verbal Learning Test	RAVLT	Verbal memory
Brief Visuospatial Memory Test Revised	BVMT-R	Visual memory
Symbol Digit Modalities Test	SDMT	Processing speed
Trail-Making Test	TMT A&B	Visual attention & executive function
Grooved Pegboard Test	GPT	Motor coordination
Wechsler Test of Adult Reading	WTAR	Premorbid functioning

The Rey Auditory Verbal Learning test (RAVLT) is a well-known neuropsychological tool that reflects a wide range of cognitive functions including immediate memory, verbal learning, and memory recall and retrieval [48]. The test is efficient in detecting memory impairments, which correspond to the left frontal lobe atrophy [49]. Moreover, Balthazar and his colleagues have suggested that the RAVLT score is significantly correlated with the left side of the prefrontal cortex, temporal, and parietal lobes [50]. The RAVLT is aslo superior in terms of diagnostic aspects. Loring's study has concluded that the RAVLT is the only test able to distinguish the localization (left or right) of temporal lobes seizure onset, in comparison with other neuropsychological instrumentations, such as California Verbal Learning Test, Boston Naming Test, and Multilingual Aphasia Examination Visual Naming Subtest [51]. In many neurological studies, the cognitive evaluations of RAVLT are often integrated with the functional

measures of brain imaging techniques to provide more comprehensive understanding about brain behavior and structure. According to Moradi, Hallikainen, and Tohka, the information detected by RAVLT scores is strongly associated with the structural changes measured by magnetic resonance imaging (MRI) in patients with Alzheimer's diseases (AD) [52]. Furthermore, the RAVLT is capable of differentiating normal aging from mild cognitive impairment (MCI) and mild AD subjects [50].

The Brief Visuospatial Memory Test Revised (BVMT-R) is a figural learning test where subjects are required to learn and retain a series of figures several times. Impaired visual memory is often correlated with the right frontal lobe deterioration [53]. Visual memory deficits in patients with the temporal lobe dysfunctions were also evidently found through information obtained from figural learning tests [54]. For instance, these tests are Rey-Osterrieth Complex figure test or Rey- O and Visual Reproduction on the Wechsler Memory Scale [54]. Benedict and his colleagues have showed that at the same given time limit, patients would rely more on their visual memory when learning multiple simple figures instead of one complex design [55]. Therefore, the BVMT-R is concluded to be more sensitive in detecting impairment than other figural reproduction tests. The BVMT-R is alsoused in conjunction with neuroimaging modalities. In the study of McIntosh and his fellows, the results have suggested that visual memory performance measured by BVMT-R is strongly correlated with structural changes of medial temporal lobe computed by MRI in older patients with metabolic syndrome [56].

Among diagnostic tests for visual attention and information processing speed, researchers frequently use Paced Auditory Serial Addition Test (PASAT) and Symbol Digit Modalities Test (SDMT). However, the SDMT, which utilizes symbols and digits to determine deficits, is more favorable and efficient due to its ease of administration and reliability of scoring. The written version of SDMT limits cultural bias and is suitable for patients with language barriers or speech disorders [57]. Two studies of

Forn and her colleagues evidenced that the performance of the screening tests for processing speed triggered a significant increase in brain activation in the occipital, temporal, and parietal brain areas [58, 59]. In addition, the study of patients with multiple sclerosis has confirmed that the scores of SDMT are highly correlated with MRI measures of atrophy than that of PASAT, making SDMT an alternative for processing speed evaluation [60].

The Trail-Making Test A&B (TMT A&B) has become a widely accepted evaluation in neurological research because of its efficacy. Each part of the test reflects different cognitive mechanisms: visuoperceptual abilities via TMT A, task-switching abilities via TMT B, and lastly, psychomotor speed via differences between TMT A&B [61]. Therefore, the trail making tests indicate the regional brain damage associated with specific task performance. Instances of this include impairments in posterior parietal areas caused by scanning deficiency measured in TMT A scores, or deficits in left dorsomedial prefrontal region and frontal areas caused by slowed shifting activity evaluated in TMT B scores [49,62]. When interpreting the TMT A&B performance, various considerable factors include age, education, mental health, and cognitive ability [63]. Understanding the causes of poor performance of TMT A&B potentially aids in determining significant diagnostics and suitable treatments.

The Grooved Pegboard Test (GPT) is a popular motor task used for measuring fine motor functions and manual dexterity. The GPT requires coordination of fingers to manipulate the objects in a timely manner. The test is administered with dominant and nondominant hands, allowing the evaluation of brain lateralization. Previous studies have shown that the GPT is more sensitive in detecting motor slowness in comparison with other assessment tools, for example, the Purdue Pegboard test and the Finger Tapping Test [64]. Moreover, extensive research has proposed that information provided by the GPT scores is not only limited to motor functions, but

also associated with other cognitive mechanisms, including memory, vision, and attention [64,65]. Due to its utility and versatility, the GPT is suitable for patients with a variety of neurological conditions, ranging from motor deterioration in Parkinson's disease to brain damage after cardiac surgery [65, 66].

The Wechsler Test of Adult Reading (WTAR) is a robust word pronunciation task that provides appropriate estimates of premorbid intelligence (IQ). The test consists of 50 words with irregular pronunciations, and its purpose is to minimize the subject's ability to apply the standard pronunciation rules while accessing knowledge prior to brain injury or disease [67]. In the early study of patients with traumatic brain injury, the results have indicated that the WTAR is more stable than the Vocabulary test and Matrix Reasoning, making it the most valid test for estimating premorbid IQ [68]. The validity of WTAR has been investigated but still remained unclear because of inconsistent findings across mulptile studies. Regardless, the WTAR is widely accepted as a valuable measure of premorbid IQ in neurological research because of its simplicity and stability [69].

CHAPTER FOUR

Instrumentation

In this chapter, fundamental fNIRS devices (Section 4.1) and experimental instrument (Section 4.2) are discussed along with the introductions of necessary software for data recording and processing.

4.1 Basic Devices of fNIRS

In general, fNIRS systems are composed of three major components: light sources to emit light, photodetectors to capture the transmitted light, and optical fibers to guide the light to/from the head.

4.1.1 Light Sources

As mentioned, two or more wavelengths of light sources are selected in the NIR spectrum, where light absorption is low due to scattering properties of biological tissues. High optical power theoretically not only increases the transmitted light through tissues, leading to a higher SNR, but also allows the use of longer SD distance, resulting in a greater penetration depth [8]. The power of the light emitters, however, should be about 5-20 mW or below to prevent tissue heating, which may distort fNIR signals and pose potential risks of scalp irritation [45].

Laser diodes (LDs) and light emitting diodes (LEDs) are the most common types of light sources used in the fNIRS instruments, and each has advantages and disadvantages. A comparison between LDs and LEDs is discussed in a paper by Scholkman. LEDs, based on spontaneous emission, emit incoherent light with a broad spectrum of 20-50nm. On the contrary, LDs, based on stimulated emission, produce coherent and monochromatic light with a narrower spectrum [8]. Compared to LEDs, LDs have a narrower operating range and limited choices of wavelength

selection. Considering that the absorption spectra of Hb is at 760nm, LDs between 695 nm and 775 nm are relatively expensive [8]. In contrast, LEDs are available at small size with a large variety of wavelength options [45]. It is also important to notice that LDs often emit higher power output than LEDs and hence require higher safety protection to prevent eye damage for both the administer and the subject [8]. Due to its simplicity and ease of use, LEDs are more favorable for portable fNIRS systems.

4.1.2 Photodetectors

The collected light has relatively low intensity. In theory, the higher the gain, the more the system amplifies the signal. Therefore, the ideal photodetector should have high internal gain to increase the intensity of the collected light. However, other factors such as device size, voltage supply, dynamic range, and photon counting speed also play an important role in the selection of detectors.

The photomultiplier tubes (PMTs), photodiodes (PDs), and avalanche photodiodes (APDs) are three types of photodetectors often used in fNIRS instrumentation. These photodetectors operate based on the photoelectric effect. Upon photon absorption in a photocathode (external) or by a semiconductor junction diode (internal), free carriers, often electrons, are emitted and can be detected as electrical signals [8].

Among the three photodetectors, PMTs, based on the external photoelectric effect, provide the highest gain (up to 10^7) with high photon counting speeds [8]. Despite these advantages, PMTs are large, sensitive to magnetic fields, and susceptible to ambient light exposure. In fact, PMTs are not as commonly employed as the other two devices because the PMT detectors require a high voltage supply and voltage stabilization [8].

Unlike PMTs, PDs and APDs, based on the internal photoelectric effect, are resistant to magnetic fields and robust to ambient light. PDs are small, compact, and easy to use and have a high dynamic range of 100 dB [70]. Since PDs have no internal

gain, the devices utilize low voltage supply and do not require voltage stabilization; instead, an external amplification is needed to amplify the signals [8]. Similar to PDs, APDs come in small to moderate packages. The APD, however, is faster and more sensitive than the simple PD because it has a moderate internal gain, ranging from 10 to a few 100, with a dynamic range of 60 dB [70]. This also means that APDs require higher operating voltages than PDs, but lower than the voltage required for PMTs.

In general, there are three main types of noises present in photodetector systems: shot noise, dark current, and thermal noise. Shot noise arises from current fluctuations caused by the stochastic nature of generated electrons [8]. It is proportional to the square root of the detected photons. By shielding the detector from background light, shot noise can be significantly minimized. Another type of noise is the dark current in which electrons are excited by the thermal energy, instead of the light energy [8]. It can be reduced by cooling the device, which is required for PMTs and APDs. Thermal noise results from thermal motion of electrons [8]. Compared to shot noise and dark current, thermal noise is relatively small and therefore can be neglected.

4.1.3 Probes

In fNIRS technique, the optical fibers are often utilized to transport the emitting light from the sources to the head, as well as carrying the existing light from the head to the detectors [8]. Even though the optic fibers provide flexibility for geometrical probe design, there is potential losses in light transmission due to fibers coupling.

4.2 Experimental fNIRS Instrument

NIRx Headgear kit from NIRx Medical Technologies LLC (Berlin, Germany) includes two main components: wearable neuroimaging caps and optode holders. The

NIRScap is similar to an EEG cap with prefixed optode positions in standard layout such as an international 10-20 system [9]. It can be partially or fully populated with optode holders, which are used to secure optodes at those prefixed positions (Figure 4.1a). Other accessories such as cable organizers and strain-relief arms are used to organize the detector cables and relief mechanical strain caused by the weights of those cables.

Once optode patterns and channel locations are determined, an optode configuration or a montage is created. The montage can be varied between studies since it is designed based on the regions of interest and the constraints of the study.

4.2.1 Imaging Instrument

The commercial CW NIRScout Extended or NIRScoutX from NIRx Medical Technologies LLC (Berlin, Germany) is the highest density fNIRS imaging system and has up to 64 sources and 32 detectors, allowing a maximum of 2048 possible channels for data collection (Figure 4.1b). In addition, NIRScoutX can be used for multi-modal measurement with other systems, for instance, EEG and fMRI. The system is connected to the host PC via a 2.0 cable. Each LED emits light at two fixed wavelengths: 760 nm and 850 nm, and its emission power per wavelength is about 5mW with a 0.01 second illumination [9]. Each bundle of source wires consists of eight dual wavelength LED emiters. The detectors used in the NIRScout are silicon PDs, which are sensitive at <1 pW with a dynamic range of 90 dB [9]. The detectors are connected to optical fibers for light transmission from/to the head. Each detector bundle has four fiber optic cables. Instead of standard single tipped optodes, dual tipped optodes are utilized in this study (Figure 4.1c). They yield high sensitivity, fasten setup procedure, and provide patient's comfort [9]. The computer cart is an essential accessory for instrument transport.

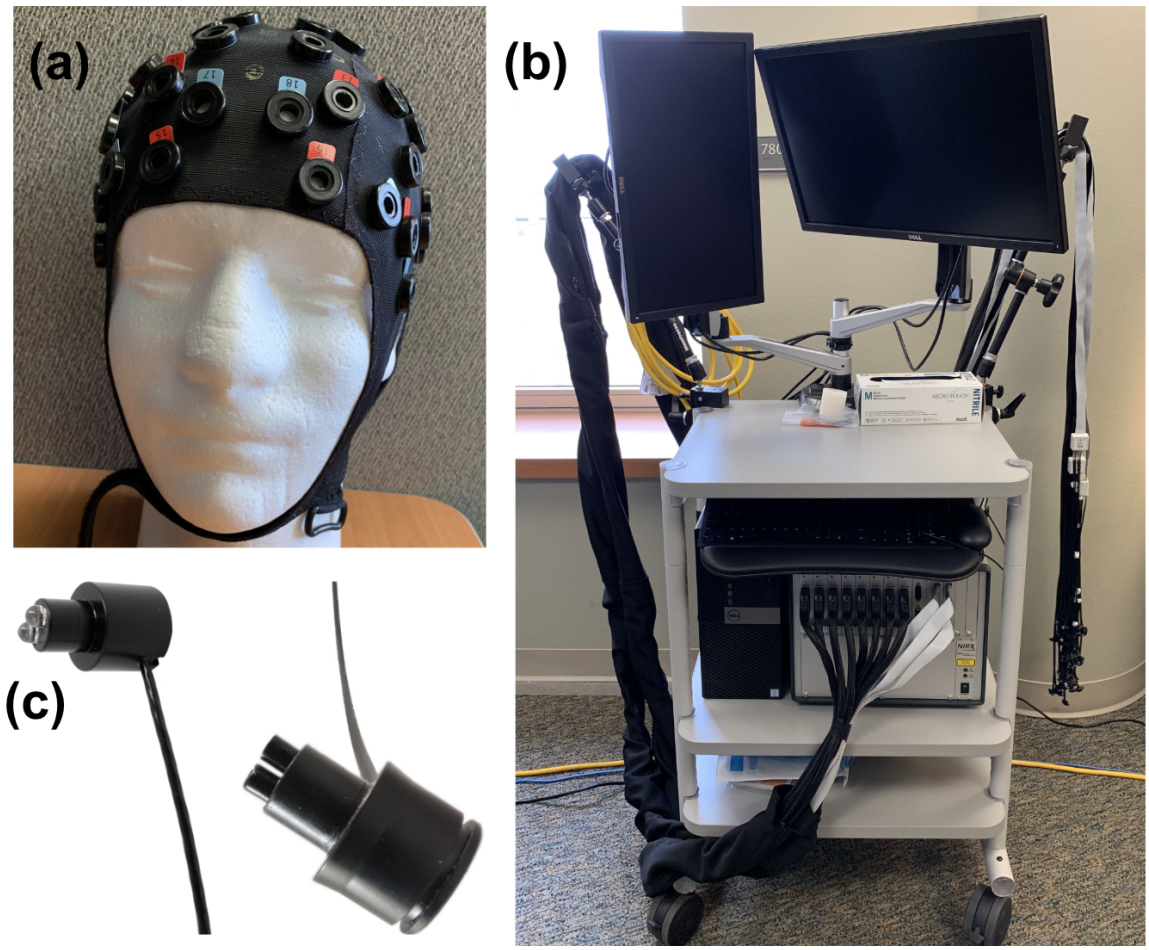

Figure 4.1. (a) NIRScap populated with optode holders, (b) dual tipped LED sources (left) and SiPD detectors (right) [9], (c) NIRScoutX imaging system

4.2.2 Data Acquisition

NIRStar (v.15.0, NIRx Medical Technologies LLC, Berlin, Germany) is the NIRScoutX data acquisition software that records and displays ultimate real-time visualization of collected data, presented in $[HbO_2]$ and [Hb] information. Before recording data, it is important to perform a calibration, so that the system can automatically adjust the gain level for each source-detector (SD) combination. If the raw signals of the channel fall below or above the optimal signal range, 0.09 - 1.4 V, the channel will receive an increase or decrease in amplification gain, respectively [71]. An indicator for signal quality, or SNR, is available for each channel and shown in Figure 4.2. Green indicates that channels receive strong hemodynamic signals and

thus require low amplification gain values, from 1-6. On the other hand, channels that detect insignificant hemodynamic signals are marked red and amplified with higher gain values from 7-8 [71]. Higher gain value is associated with lower SNR; therefore, gain level is a crucial factor when determining channel's quality and analyzing data. After calibration, the system is ready for data recording, and collected data is saved in a format compatible with NIRx's analysis software such as nirsLab and also other available toolboxes such as Homer2, NIRS-SPM, or NIRFAST [8].

Signal Quality	NScout Gain [10^x]	Level [V]	Noise [%]
Excellent	1 - 6	0.09 - 1.40	< 2.5
Acceptable	7	0.03 - 0.09 1.40 - 2.50	2.5 - 7.5
Critical	0 8	0.01 - 0.03 > 2.50	> 7.5
Lost	-	< 0.01	-

Figure 4.2. Signal quality scale for fNIRS channels

In general, NIRStar allows users to determine illumination sequence, indicating the order of sources to turn on during each sampling process. Based on the spatial arrangement of optodes, users can create the probe setup file for subsequent data analysis, as well as defining the corresponding topographic layout for data visualization. Furthermore, 8 event trigger ports and manual markers are available for synchronizing the data with external time [71].

4.2.3 Data Processing

The nirsLAB (v2017.06, NIRx Medical Technologies LLC, Berlin, Germany) package is a MATLAB-based software analysis tool that is highly compatible with time-series data obtained from NIRScoutX and other instruments such as NIRSport or DYNOT imaging systems [10]. To begin data processing, nirsLAB requires an input of raw-NIRS measurements along with information regarding probe locations

and experiment timings. The toolboxes implemented in nirsLAB provide basic data pre-processing functions, including: 1) excluding irrelevant time intervals; 2) removing discontinuity and spikes; 3) detecting saturation; 4) evaluating the quality of the raw measurements; and 5) deleting irrelevant frequency band [10].

In this study, the raw data acquired from intraopetrative fNIRS recording is processed using the following nirLAB modules: signal quality check, frequency filtering, and computation of hemodynamic states. Signal quality of each fNIRS channel is presented in the form of a heatmap with a color-coding scale. As shown in Figure 4.3, the y axis is source number, and the x axis is detector number. Each fNIRS channel index is labeled with numbers inside the map; in this example, there are 44 channels. Red indicates high value of amplification factors from 7-8, while blue represents low value of gain from 2-5. Typically, channels with high amplifications

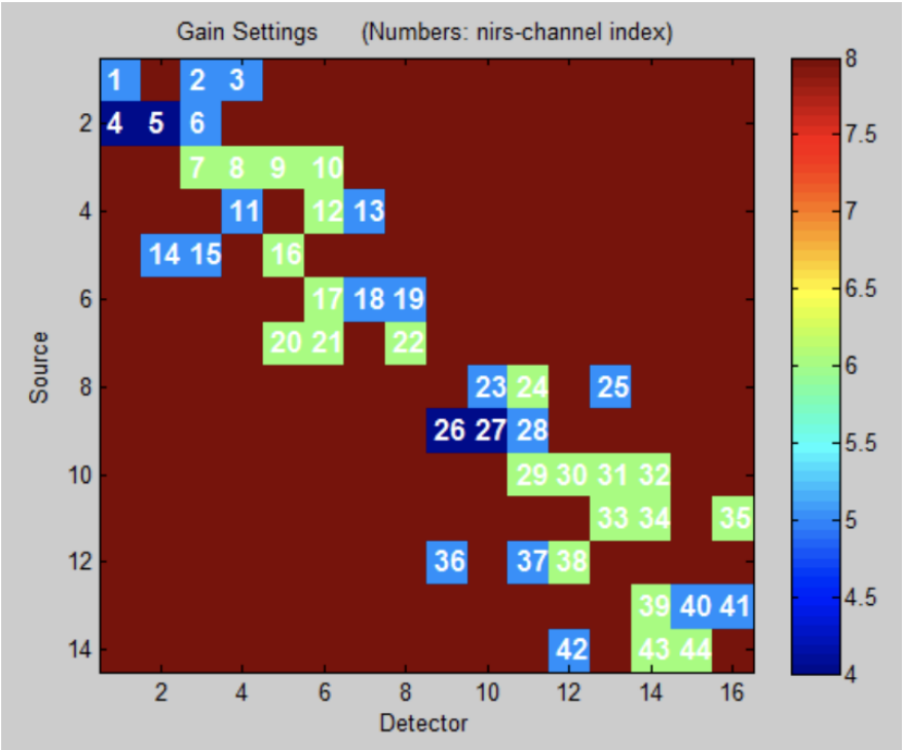

Figure 4.3. An example of a gain map, generated in nirsLAB and used to check quality of acquired signals via amplification levels. Red indicates high gain (7-8), and blue indicates low gain (2-5) [10]

are often classified as 'weak channels' due to an insufficient measured hemodynamic response. Despite this factor, all channels must be examined with other measures to determine whether there is potential hypoxia occurred within the corresponding brain regions. Afterwards, a band pass filter is applied to remove artifacts and preserve wanted signals. The filtered data is then computed into hemodynamic states, including oxygenated [HbO_2] and deoxygenated [Hb] hemoglobin concentration changes with respect to the input baseline. Relative changes of oxygenated [HbO_2] and deoxygenated [Hb] hemoglobin concentration are extracted from nirsLAB and further analyzed in Matlab. The processing code is developed to identify and replace outliers, as well as performing one-sided t-test, a statistical test to detect potential hypoxic events that happened during cardiac surgery.

CHAPTER FIVE

Methodology

A brief description of surgery types is discussed in Section 5.1. Figure 5.1 presents an overview of the experimental design. The study consists of three time points: prior to surgery, surgery, and subsequent to surgery. There are two main parts of the study: fNIRS imaging technique (Section 5.2) and neurocognitive assessments (Section 5.3). The following sections explain the procedures used in each part in great detail. The clinical informed consent form, demographic screening survey, research protocol outline, and neurocognitive measures are approved by Institutional Review Board (IRB) at Baylor Scott and White Medical Center, Temple TX. The IRB number of the study is 017-409.

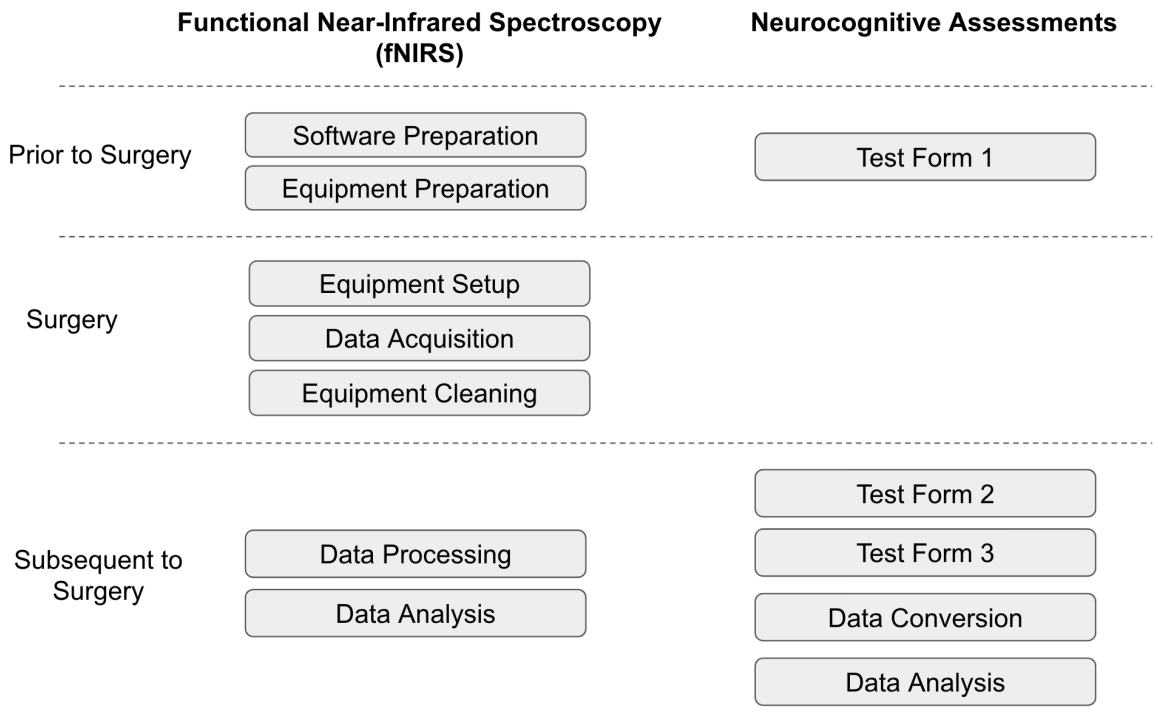

Figure 5.1. An overview of the experimental design of the study, consisting of two main parts: fNIRS imaging technique and neurocognitive assessments

5.1 Cardiac Surgery

Four different types of cardiac surgery were included in this study: coronary artery bypass grafting (CABG), transcatheter aortic valve replacement (TARV), aorta ascending graft and root replacement, and endovascular aortic aneurysm repair (TEVAR). During an open-heart procedure, except TEVAR, the heart was temporarily stopped and connected to CPB device to maintain the circulation and regulation of blood [35]. The surgical duration varied from 3-4 hours for normal cases and up to 5-6 hours for very complex cases [35]. During an open-heart surgery, patients received general anesthesia and lay supine on the operating table. For comfort, the patient's head rested on a doughnut-shaped cushion to keep the neck in a natural position. These factors significantly influenced the design of the montage, cap placement, intraoperative equipment setup, and data recording process.

5.2 Functional Near-infrared Spectroscopy (fNIRS)

5.2.1 Prior to Surgery

5.2.1.1 Software preparation. The main monitored regions of the brain were prefrontal and frontal lobes; in addition, a portion of temporal and parietal lobes was included in the probe design. Due to the patient's position during surgery, data collected from occipital lobes might yield poor quality and low accuracy. The probes at these regions might also cause discomfort and skin irritation after long duration. Therefore, occipital lobes were not monitored in this study.

As mentioned in Section 4.2, NIRScoutX was employed as an imaging instrument while NIRStar was used as the user-interface. In an attempt to cover the regions of interest, 20 sources and 24 detectors with 46 measurement channels were utilized. With the interoptode distance of 2.5 cm, these optodes were arranged in the international 10-20 EEG system (Figure 5.2a). The montage used in the current

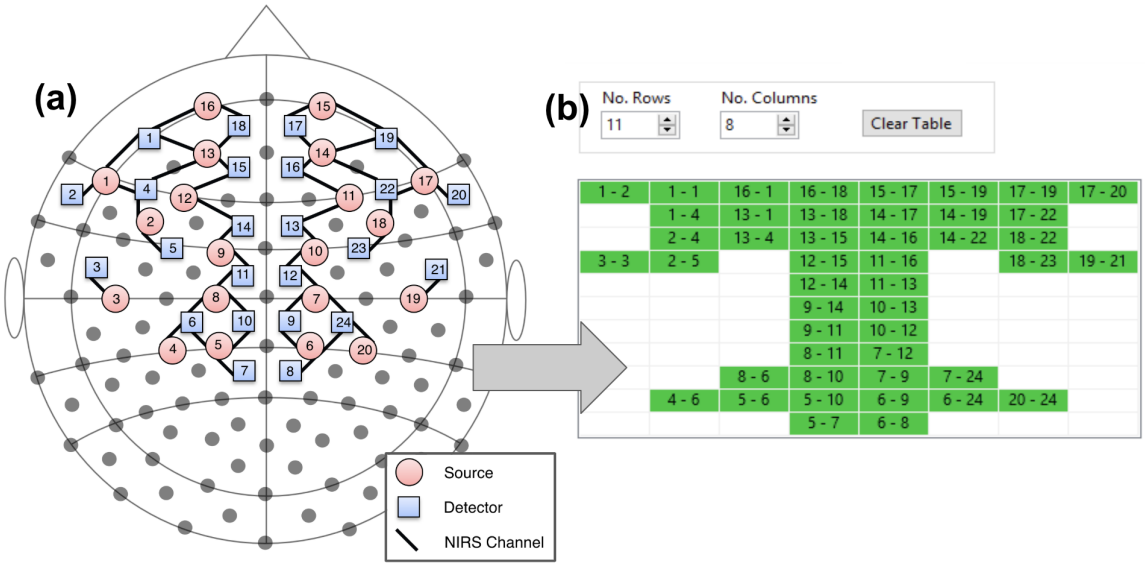

Figure 5.2. (a) fNIRS montage with 20 sources and 24 detectors arranged in 10-20 international system, (b) topographic layout generated in NIRStar for data visualization

study was developed by Dr. Haleh Aghajani, a postdoctoral scholar at Baylor Scott and White Medical Center, Temple TX.

In NIRStar, a probe setup file was simply created by specifying numbers of sources, detectors, and channels and translating the physical optode arrangement onto the 2D head figure in the module. Similarly, a corresponding tomographic layout (Figure 5.2b) was generated for data visualization. Figure 5.3 presented the illumination sequence of 20 LED sources used in the study. The rows were sequential steps, and the columns were source numbers. For each step, paired sources were located at least 6 cm apart from each other to avoid cross-talk [71]. The study utilized 7 steps per sampling process. Based on the number of steps, the sampling rate was 8.929 Hz. This sampling rate was determined by the following Equation 5.1 [71]

$$f_{sampling} = \frac{62.5Hz}{no.of steps} \tag{5.1}$$

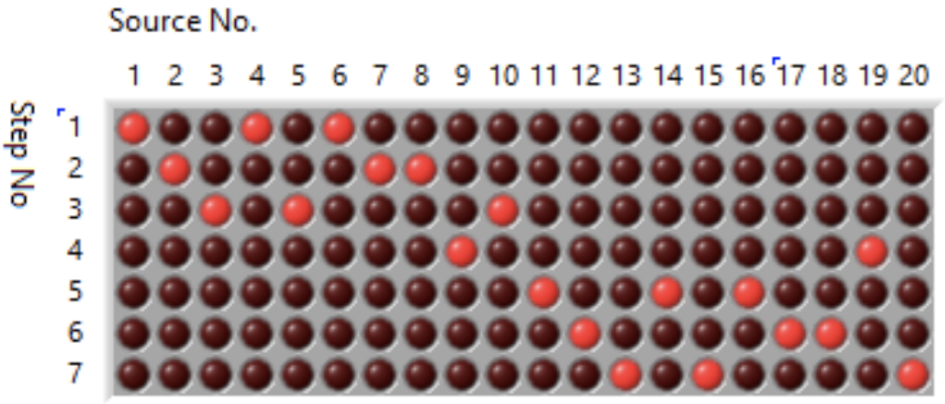

Figure 5.3. Illumination sequence for 20 LED sources

5.2.1.2 Equipment preparation. Based on the montage, optode holders and numerical label tags were placed on the NIRScap. Red tags were dedicated to sources, while blue tags were dedicated to detectors. To suit a wide range of intended users, NIRScaps were available in different sizes: 54 cm for small, 56 cm for medium, 58 cm for large, and 60 cm for x-large. A cap that was bigger or smaller than subject's head resulted in patient's discomfort and invalid measurements. Therefore, finding the most suitable NIRScap for each subject was essential. A NIRScap size was selected based on the measurement of the subject's head circumference. A rubber measuring tape was wrapped from the forehead to the back of the head, measuring the widest circumference.

Due to the doughnut-shaped cushion and the patient's position during surgery, placing the fiber optic cables and source wires at the back of patient's head was not ideal because this position tilted the optodes and tightly bent the cables. More importantly, it caused patient pain and even bleeding on the scalp toward the end of the surgery. As a result of many discussions with Dr. Haleh Aghajani and practices under Dr. Daniel Lee's supervisions, it was concluded that the fiber optic cables and source wires should be equally branched out to both side of the head (Figure 5.4) in order to maximize patient's comfort, obtain reliable data from correct optode

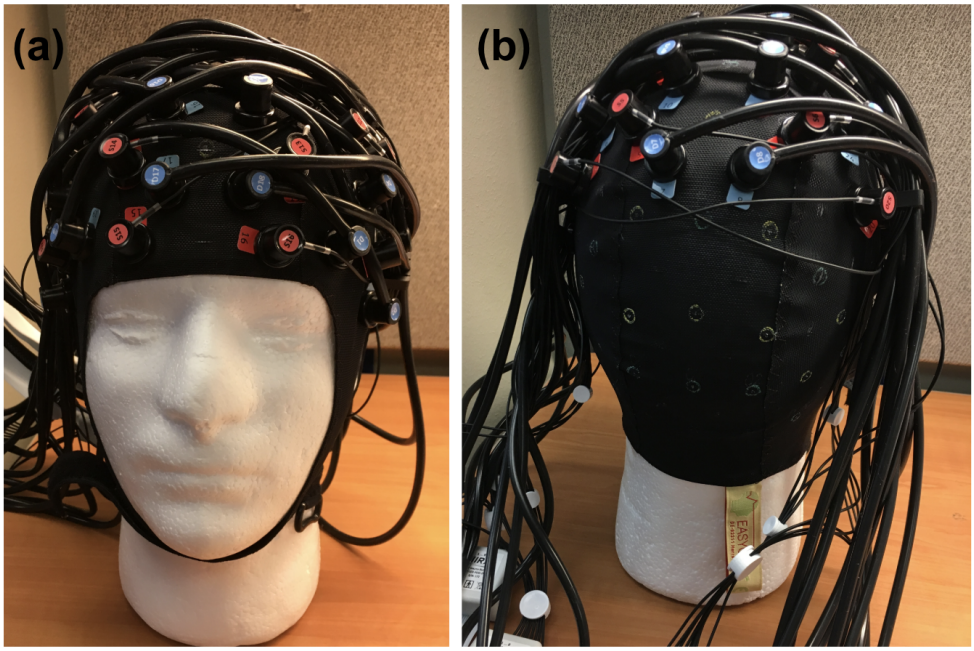

Figure 5.4. (a) Front and (b) back view of NIRScap after coupled with sources (red tags) and detectors (blue tags). The yellow tag at the back of the cap was an important element for the cap placement, discussed in Section 5.2.2.1

positions, and prevent instrument damage from tight cable bending (bending radius <2 cm) [9].

In addition, two cable organizers were placed on each side of the cap to direct the routing of the cables, avoiding undue torque and tipping of the optodes. Applying a small amount of baby oil on the q-tip and rubbing it inside the optode holders allowed optodes to smoothly fit into the holders. This prevented accidental damages on optodes during the placement process. While placing the optodes into the corresponding holders, users avoided crisscrossing the fiber optic cables and source wires. As the fiber optic cables were properly attached to the cable organizers, they did not exert pulling pressure onto the optodes; the movements of those cables or subject movements also did not change the optode positions [9]. The NIRScap coupled with probes was then placed in a clean plastic bag and ready for the experiment.

5.2.2 *Surgery*

Approximately 2 hours prior to the patient's arrival, NIRScoutX cart and NIRScap were brought to the OR. An overview of intraoperative fNIRS monitoring technique utilized in the study was illustrated in Figure 5.5. Before entering the OR, research assistants communicated with surgical staff to ensure safety while transporting the cart in and out of the OR. The cart was often located behind the anesthetic monitoring devices and hence relatively close to the surgical site, making it possible to access the patient's head. Once the cart was in the OR, the NIRScoutX was powered up, and NIRStar was loaded with predefined configurations to be ready for intraoperative recording.

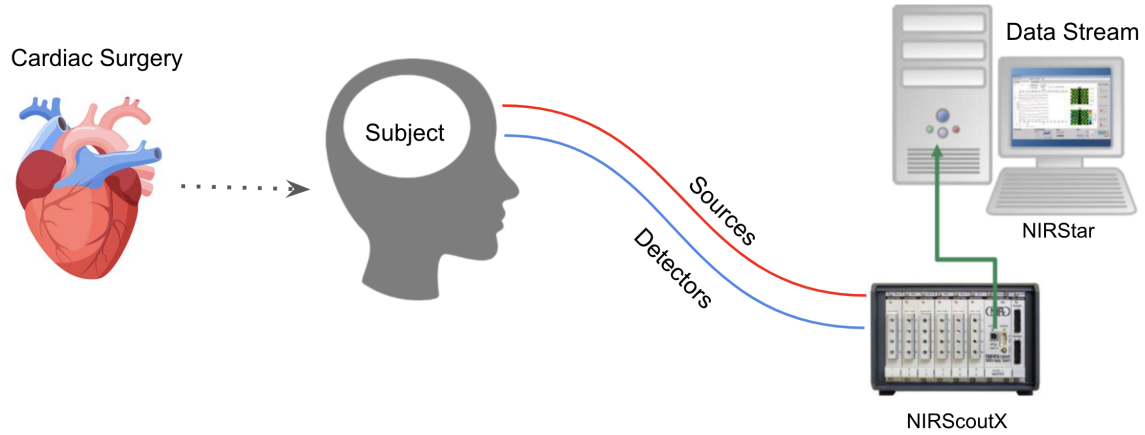

Figure 5.5. Intraoperative fNIRS recording layout. While the surgeon operates on the patient's heart, NIRScoutX measures hemodynamic response and transmits measurements to NIRStar for data visualization and data recording in real-time (Images adapted from NIRx [9])

5.2.2.1 Equipment setup. After the patient was completely anesthetized, the cap placement procedure began. Cap placement was a critical factor in determining the reliability and quality of fNIRS signals. Precise placement of the cap not only allowed maximum skin-optode contact, but also ensured good measurements at the exact regions of interest. The position of the cap on the patient's head defined the optode locations, which were relevant to local brain regions [72]. A cap slanted

to one side produced unreliable data because it deviated spatial optode positions. The cap, therefore, was required to equally cover both sides of the head and was adjusted accordingly to the patient's skull contour. However, placing an NIRScap coupled with probes on an anesthetized patient was a complex procedure. It required a synchronized coordination of two research assistants. After many trials under Dr. Lee's supervision and with the assistance of Dr. Aghajani, the cap placement technique was developed.

The first person slid one hand behind the patient's neck with a yellow cap tag on at least three fingers to secure the cap at the nape of the patient's neck. Meanwhile, the other hand of the first person was placed underneath the patient's head to lift it up, leaving enough space for the second person to pull the cap over the head. As the second person pulled the rest of the cap towards the patient's forehead, the first person removed the hand that supported the back of the patient's head. As the cap covered the patient's head, the research assistant carefully adjusted the cap and gently placed the ears on the side slits to make the cap fit snugly on the scalp. When the NIRScap was properly positioned, the research assistant slightly pushed each optode onto the scalp, passing through the patient's hair to allow maximum light penetration.

Throughout the stages of the study, the intraoperative fNIRS setup rapidly changed to adapt to the OR setting, improve patient's comfort, and importantly, obtain high signal quality. After Dr. Randal Babour, a founder of NIRx Medical Technologies LLC (Berlin, Germany), offered constructive feedback regarding the neuroimaging setup, an overcap and an articulated arm were integrated into the setup to minimize background light and improve signal quality. An overcap was placed over the NIRScap to reduce ambient light. Meanwhile, an articulated arm with a cable clamp, attached beneath the operating table, was necessary to secure the cables and wires, prevent tight cables bending, and reduce pulling pressures exerted on patient's

head. With the use of these components, the system became more robust and resistant to motion. To enhance safety, the cables and wires were carefully bent at a wide angle, wrapped in disposable OR towels, and secured with tapes. This maintained a neat and safe workstation for anesthesiologists and prevented slips and trips on the cables. Figure 5.6 presented an overview of fNIRS equipment setup in the OR. Proper setup

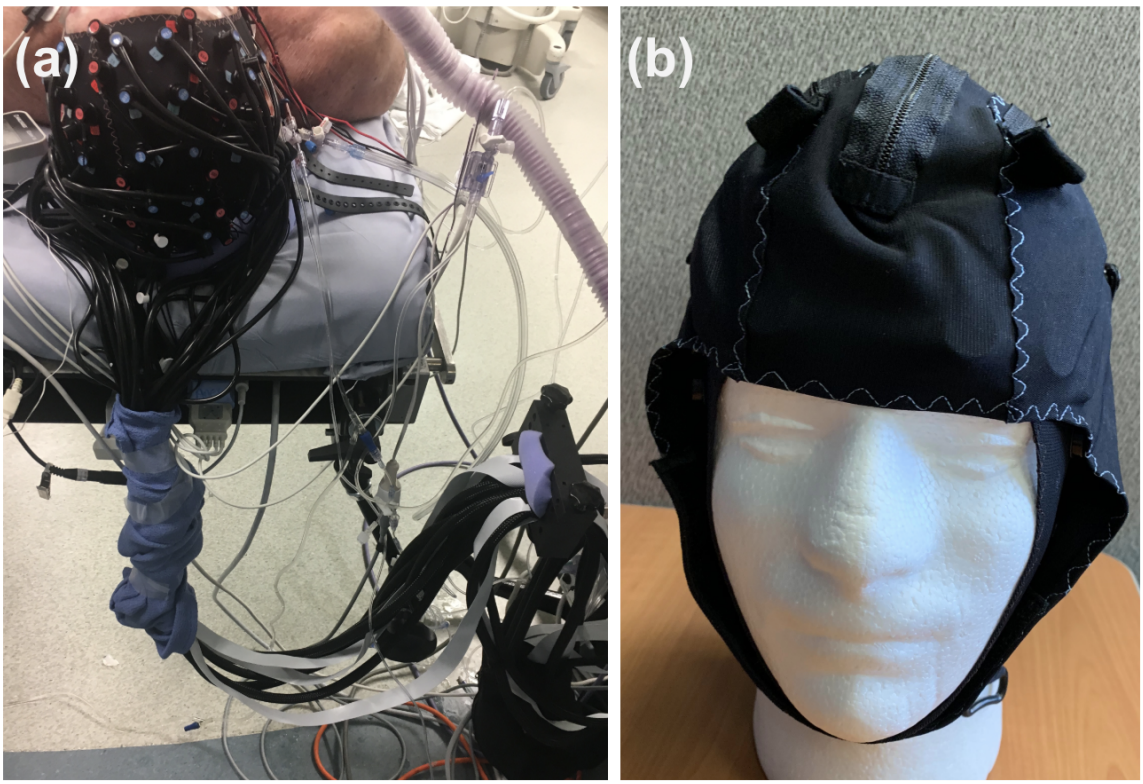

Figure 5.6. (a) NIRScap is placed on the patient's head, and fibers cables are secured by a strain-relief arm, (b) an overcap is placed over the NIRScap to prevent ambient light

of cap and cables allowed an adequate amount of time for research staffs to perform calibration on NIRStar. If needed, optodes were fixed for better contact with skin, and the system was calibrated again.

5.2.2.2 Data acquisition. Once calibration was done, continuous fNIRS recording started. The recording began at least 5 mins prior to the first incision to obtain the baseline measurements, which were critical values for data analysis. The

longer the recording prior to the first incision, the more accurate baseline measurements.

During an intraoperative period, surgeons called out surgical events as they happened. For instance, "time in" meant first incision was performed on the patient's chest; "bypass on" meant the patient's heart was connected to the CPB; and "take the venous" meant the patient's heart was disconnected from the CPB. These events were marked on the NIRStar by using trigger ports and recorded in the OR event log, where additional information such as time, frame number, and mean arterial pressure (MAP), was documented for data analysis. Other events like motion artifacts, which caused drastic changes in fNIRS data, were also observed and recorded accordingly.

During fNIRS recording, motion artifacts resulted from various factors that disturbed fNIRS signals. For example, while monitoring the patient's vital signals, anesthesiologists accidentally moved the head, affecting skin-optode contact; or while performing skin preparation, surgical staff raised the patient's legs up, increasing blood flow to the head. Researchers, therefore, continuously monitored the fNIRS data, paid close attention to these unavoidable and unpredictable events, and recorded them in the NIRStar and OR event log.

5.2.2.3 Equipment cleaning. At the end of fNIRS recording, the overcap, NIRScap, and strain-relief arm were removed from the the patient's head and the surgical table. The cleaning procedure in Appendix B was often executed when most of the patient's chest cavity was closed, indicating the completion of surgery. It was very important to disassemble optodes from the cap before cleaning equipment to avoid damages caused by inappropriate cleaning agents.

After every intraoperative fNIRS recording session, the equipment cleaning procedure was performed to maintain high hygiene. Two sections were included in this procedure, one for imaging devices and the other for the NIRScap. The device cleaning procedure (Appendix B.1) was developed based on Dr. Aghajani's suggestions and

NIRx NIRScout User Manual [9]. Performing the procedure thoroughly reduced the possibility of physical damages to the fiber optic probes, which were made of delicate and fragile optical fibers. For the NIRScap, the routine cleaning (Appendix B.2.1) and deep disinfection (Appendix B.2.2) were adapted from the instructions of EEG cap cleaning [73]. To maintain the cap elasticity and its shape, researchers gently washed the cap in a circular motion and thoroughly cleaned it with cold water to remove blood residuals. Sekusept, a well-known solution for disinfecting EEG caps, and its use for the NIRScap disinfection was confirmed by the NIRx Support Team.

5.2.3 Subsequent to Surgery

5.2.3.1 Data processing. The raw data was loaded into nirsLAB along with the NIRStar event logs and probe setup file. All data at all the time points were completely preserved. Each channel was evaluated via gain map. The higher the gain, the lower SNR. Therefore, channels with high gain were classified as 'weak channels'. The classification of strong and weak channels was a considerable factor for data analysis. In order to remove noise and artifacts, a bandpass filter with a frequency range of 0.01-0.5 Hz was applied to the raw data. A high cut-off of 0.5 Hz was used to eliminate high frequency instrumental noises and cardiac activity, which was approximately 1 Hz [43]. Low-frequency physiological signals and residual long-term drifts from fNIRS imaging instrument were reduced with a cut off of 0.01 Hz [74]. After frequency filtering, the hemodynamic states were computed using the MBLL in nirsLAB. The parameters were as follows: interoptode distance was 2.5 cm; DPF1 was 7.25 at 760 nm; and DPF2 was 6.38 at 850 nm. The baseline was determined with 75μM of total hemoglobin and 65% of $[SvO_2]$. The relative changes of oxygenated $[HbO_2]$ and deoxygenated [Hb] hemogoblin concentration with respect to the baseline were exported as ASCII files. The exported data was then imported into Matlab for further processing.

5.2.3.2 Data analysis. Previous studies suggested that hypoxia was defined as more than 20% decline in oxygen saturation from the baseline [18, 75]. This simply meant that oxygen level should maintain at least 80% of the baseline values. Moreover, oxygen desaturation within 2 minutes could cause cell injury and cell death [76]. Continuous hypoxia more than 3 minutes could lead to irreversible brain damage and eventually cognitive deficits [76]. Consecutive duration of hypoxia was indeed important in determining potential cerebral damage, resulting in cognitive declines. Therefore, one minute was a rational sampling interval for computation. Furthermore, multiple consecutive periods of 1-minute interval indicated prolonged hypoxia and thus provided a reasonable warning for the need of interventions.

Using the exported data from nirsLAB, a ratio of relative changes of oxygenated [HbO_2] and deoxygenated hemoglobin [Hb] was calculated using the developed processing code in Matlab. Assuming oxygen supply remained constant, a decrease in this ratio corresponded to an increase in oxygen consumption of tissues. As the ratio fell below 80% of the baseline, it indicated oxygen deprivation, which potentially led to hypoxia. Therefore, this ratio could serve as an indicator for potential hypoxic events.

The data was divided into two time intervals: baseline and bypass duration. Baseline measurements were established from the beginning of the recording session to the first incision on the patient's chest. On the other hand, a period in which the patient was on the CPB machine was defined as bypass duration. The mean of the baseline was then computed. At baseline, outliers were detected within a mean $\pm$ 5 standard deviation and replaced with a mean value of a 10 second window, consisting of 5 seconds above and 5 seconds below the outlier. Sudden changes in fNIRS signal that pass the cut-off threshold most likely result from extreme noise rather than hemodynamic response. After detecting and replacing outliers in baseline measurements, 80% of the mean values were calculated. The bypass period was divided into

1-minute intervals. One-sided t test was performed between 80% mean of the baseline and the data obtained in 1-minute interval across all 46 channels. The purpose of this analysis was to detect potential hypoxia that happened during cardiac surgery and investigate whether hypoxic events corresponded to brain regions associated with cognitive declines. Based on the statistical test, detection of oxygen desaturation was identified if the ratio dropped below 80% mean of the baseline. Within each channel, the total number of oxygen desaturation were defined as 'detection times'. Two consecutive detections of oxygen desaturation were specified as '2-minute interval'. Similarly, three consecutive detections of oxygen desaturation were specified as '3-minute interval'.

5.3 Neurocognitive Assessments

5.3.1 Test Battery

In this study, the test battery was selected by Dr. Crystal Lantrip, a psychologist from Baylor Scott and White Medical Center, Temple TX, in accordance with Dr. Lee. After several training sessions with Dr. Jared Benge, a neuropsychologist from Baylor Scott and White Medical Center, Temple TX, research assistants were well-prepared to independently administer the neurocognitive assessment. Each neurocognitive session was given to a single subject working with a trained examiner in a quiet environment. This allowed the subject to be free from any distraction that might disturb their flow of thoughts and concentration while taking the tests. The subject's responses were then recorded by the examiner.

The assessment usually lasted up to 45 minutes; however, the finishing time and the test completion were dependent on various factors, ranging from external distractions to individual's cognitive abilities and state of health. Within the test duration, the examiner provided an additional break period upon the subject's request. In the case where the assessment was completely terminated, it was considered

'incomplete'. On the other hand, the assessment was defined as 'missed' when it was not performed within the proposed timeline. Three test forms (Test Form 1, Test Form 2, and Test Form 3) of the neurocognitive assessment were given at three respective time points: prior to surgery, hospital discharge, and the first follow-up clinic visit.

WTAR was only included in Test Form 1, and each test form had different RAVLT and BVMT-R versions to reduce practice effects. The rest of the test battery and the order of each neurocognitive measure in the battery remained the same for all three forms. As a result of a few trials with patients and several consultations with Dr. Benge, the order of the neurocognitive measures in the battery was presented in the following sequence:

(1) RAVLT
(2) TMT A&B
(3) SDMT
(4) BVMT-R
(5) RAVLT Delay
(6) GPT
(7) WTAR
(8) BVMT-R Delay

RAVLT was the longest test and required about a 20 minute delay; therefore, it was placed as the first test for time management. SDMT, which involved symbols and numbers, was placed before BVMT-R, which involved complex figures, to prevent an interference effect with BVMT-R delay test. The other tests were assigned in the order to fulfill the delay time of RAVLT and BVMT-R.

5.3.2 Prior to Surgery

The first neurocognitive assessment, considered as the baseline of the subject's cognitive performances, was given on the day that patients signed the study consent or

within one week prior to surgery. At the beginning of the assessment, the subject was required to fill out a demographic survey, including basic questions relating to age, race, ethnicity, gender, education, smoking habits, alcohol consumption, etc. This survey was needed for data analysis. The subject's head circumference was measured for an appropriate NIRScap size selection. After the completion of these tasks, Test Form 1 was administered to the subject.

5.3.3 Subsequent to Surgery

The second neurocognitive assessment was given on the date of hospital discharge. The discharge date was approximately 7 days after surgery, but could vary depending on the individual's recovery process. At this stage, Test Form 2 was performed. Test Form 3 was given at the first follow-up clinic visit, approximately three weeks to a month after the surgery date. In theory, the third neurocognitive assessment provided more accurate results because the side effects of anesthesia and medications were minimized by this point.

5.3.3.1 Data conversion. For RAVLT, BVMT-R, and WTAR, the raw scores were defined as the numbers of the subject's correct responses, while the subject's cognitive performance was measured based on the completion time of tasks in TMT A&B, SDMT, and GPT. The raw scores were compared to normative data, a baseline distribution established by a representative sample of defined population [77]. Depending on neurocognitive tests, normative data was selected based on subject's demographic characteristics, for example, age, ethnicity, education, and/or handedness. The raw scores were transformed into standardized scores: Z scores for RAVLT and SDMT and T scores for BVMT-R, WTAR, TMT A&B, and GPT. Z scores were generated in Equation 5.2

$$Zscore = \frac{(Patient'sRawScore - NormativeSampleMean)}{NormativeSD} \tag{5.2}$$

where mean (M) and standard deviation (SD) were from demographically matched normative data. For the purpose of data analysis, all T scores (M =50, SD =10) are converted to Z scores (M =0, SD =1) using a psychometric conversion table [78].

5.3.3.2 Data analysis. Preoperative assessments or baseline measurements were obtained from the results of Test Form 1, while postoperative assessments were derived from results of Test From 3. WTAR was mainly used to determine whether subjects were able to pronounce irregular words without prior knowledge, the scores from the test were not included in the analysis of this study. Data from Test Form 2 was not as reliable as the data from Test Form 3 because the subject's cognitive performances might be underestimated due to several factors such as sleep disturbances, anxiety, pain, and medication effects that subjects were still under influence after anesthesia and surgery [79, 80]. Since these factors negatively impacted the accuracy of the neurocognitive assessments and possibly overidentified the incidenece of POCD, the results of Test Form 2 were not reviewed in this study.

By comparing pre- and post cognitive performances at the individual level, intersubject variability was significantly minimized because subjects served as their own controls [79]. Depending on the changes in the individual's pre- and post cognitive performances, subjects were categorized into three groups for each neurocognitive test: declined, stable, and improved. Subtle cognitive deficits following cardiac surgery were identified and considered 'declined' if a reduction of Z score exceeded a cut-off of 1 SD [78]. Meanwhile, test scores were considered 'improved' if a change of Z score was about 1 SD above the baseline. If there was no significant decrease or increase with respective to the cut-off threshold, test scores were defined as 'stable'. This classification identified potential candidates for the developments of POCD following cardiac surgery. Furthermore, their fNIRS measurements might display detectable markers for adverse events happened during an intraoperative period.

CHAPTER SIX

Results and Discussion

This chapter discusses the characteristics of participants and reports two case studies through the individual's neurocognitive evaluations and fNIRS findings.

6.1 Participants

A total of 30 patients, who were considered for cardiac surgery with a cardiopulmonary bypass (CPB), enrolled with the Department of Surgery, Division of Cardiothoracic Surgery at Baylor Scott and White Medical Center in Temple, TX. Ten patients were excluded due to the following reasons: 2 for consent withdrawal, 3 for lack of fNIRS measurements and neurocognitive assessments, 3 for lack of neurocognitive measures, 1 for lack of demographic information, and 1 for pregnancy beyond the first trimester. Of the remaining 20 patients, 50% underwent CABG; 20% underwent TARV; 15% underwent Ascending Aorta Graft and Root Replacement; and 10% underwent TEVAR. Continuous fNIRS measurements of 18 of these patients were acquired during the entire surgical duration. The average duration of CPB was 132.9 mins (SD = 46.9). Furthermore, a total of 44 neurocognitive assessments, including Test Form 1 (45.4%), Test Form 2 (27.3%), and Test Form 3 (27.3%), were performed among the 20 patients.

6.2 Descriptive Statistics

In this study, cognitive performances of 12 patients who received both pre-operative (Test Form 1) and a-month postoperative assessments (Test Form 3) were reviewed. The sample included male (58%), Caucasian (83.3%), and right handed (91.7%). The mean age of the sample was 63.8 years (SD=18.4; range, 23 - 82). The mean number of years of education was 12.8 years (SD=2.2; range, 9-16).

The mean of postoperative testing intervals was approximately 29 days (SD=7.3). The postoperative testing periods, as well as the numbers of patients who received postoperative tests varied because of scheduling conflicts, patient travel, and patient's health conditions.

6.3 Neurocognitive Evaluations

In Table 6.1, cognitive performances of the 12 patients are summarized in terms of mean (M) and standard deviation (SD). For each neurocognitive test, a paired sample t-test is performed between the baseline and the first follow-up scores with a 95% confidence interval (α=0.05). The test indicates that verbal memory performance of postoperative assessments, including RAVLT total (t=-2.53, p=0.03) and recall (t=-2.32, p=0.04), is significantly lower than that of preoperative assessments. On the contrary, there is no significant difference in cognitive performances between baseline and postoperative scores for visual memory (BVMT-R; t=0.86, p=0.41), visual attention (TMT A; t=0.65, p=0.53), executive function (TMT B; t=1.33, p =0.21), processing speed of information (SDMT; t=-0.12, p=0.91), and fine motor coordination with dominant hand (GPT_DH; t=1.01, p=0.33) and non-dominant hand (GPT_NDH; t=0.62, p=0.54).

Table 6.1. Mean Performances on Neurocognitive Measures Between Baseline and Postoperative Assessments

		Presurgery		Postsurgery	
Cognitive Domain	Measure	M(Z)	SD	M(Z)	SD
Verbal memory	RAVLT Total	-0.23	1.52	-0.81	1.69
	RAVLT Delayed	0.29	1.16	-0.51	1.20
Visual memory	BVMT-R Total	-0.48	1.22	-0.19	1.14
	BVMT-R Delayed	-0.07	1.21	0.17	1.15
Visual attention	TMT A	-0.47	1.00	-0.33	0.85
Executive function	TMT B	-0.65	0.94	-0.33	1.19
Processing speed	SDMT	-0.37	0.88	-0.38	0.97
Motor coordination	GPT_DH	-1.13	0.66	-0.93	0.57
	GPT_NDH	-1.23	0.93	-1.06	1.16

Based on the postoperative evaluations, patients are categorized into three groups: declined, stable, and improved. The results can be found in Table 6.2. There is a decline in performances of verbal memory (RAVLT) and visual attention (TMT A). While processing speed of information (SDMT) remains the same after cardiac surgery, there is notable improvement in visual memory (BVMT-R) and executive function (TMT B). Within the group, performances of fine motor coordination of dominant hand (GPT_DH) are slightly declined; in contrast, fine motor skills of non-dominant hand (GPT_NDH) are improved.

Table 6.2. Postoperative Assessments

Cognitive Domain	Measure	% Declined	%Stable	%Improved
Verbal memory	RAVLT Total	25	75	0
	RAVLT Delayed	33.3	66.7	0
Visual memory	BVMT-R Total	8.3	66.7	25
	BVMT-R Delayed	16.7	66.7	16.7
Visual attention	TMT A	25	75	0
Executive function	TMT B	8.3	58.4	33.3
Processing speed	SDMT	0	100	0
Motor coordination	GPT_DH	8.3	91.7	0
	GPT_NDH	0	90.9	9.1

Generally, the statistical results are influenced by several factors. The sample size of the study is relatively small (n=12). Preoperative anxiety may underestimate the patient's cognitive performances during the first assessment, while practice effects may overestimate the performances postoperatively [80]. In order to improve the reliability of neurocognitive results, practice effects should be considered when interpreting the neurocognitive findings [80]. Since the alternate test forms cannot completely eliminate practice effects, the reliable change index (RCI) can be used to evaluate whether changes in neurocognitive functions are statistically significant [81]. Lack of interest also results in low cognitive performance; therefore, motivating patients prior to each testing session may help to reduce this effect.

6.4 Case Study

Two patients who received preoperative and postoperative assessments and had intraoperative fNIRS measurements were further discussed in this section. Table 6.3 presents their baseline and the first follow-up evaluations in Z scores relative to normative data, which is selected based on the individual's demographic characteristics.

Table 6.3. Baseline and Postoperative Performances on Neurocognitive Measures of Patient 1 and Patient 2

	Patient 1		Patient 2	
Cognitive Domain	Presurgery	Postsurgery	Presurgery	Postsurgery
Verbal memory (RAVLT Total)	0.18	0.45	-2	-3.03
Verbal memory (RAVLT Delayed)	1.48	1.48	-1.27	-2.27
Visual memory (BVMT-R Total)	0.5	0	-2	0
Visual memory (BVMT-R Delayed)	1	-0.5	-1.5	0.75
Visual attention (TMT A)	1	-0.67	-0.67	-0.33
Executive function (TMT B)	-0.25	-1.5	-0.33	0.55
Processing speed (SDMT)	-0.17	-0.17	-0.03	-0.19
Motor coordination (GPT_DH)	-2	-2	-0.75	-1.25
Motor coordination (GPT_NDH)	-2	-2.33	-0.75	-0.5

6.4.1 Case 1

Patient 1 is a 23 year old Caucasian female who underwent an aortic ascending graft and root replacement. She had long, thick hair with dark brown color. She had 12 years of education, and no clinical history of neurologic disorders or stroke was reported.

6.4.1.1 Neurocognitive analysis. At baseline, her performances of verbal memory (RAVLT), visuospatial memory (BVMT-R), visual attention (TMT A) were well above expectation. Although her execution function (TMT B) was about average, her motor coordination (GPT) was severely below average compared to age matched norms. At 36 days post surgery, measures of verbal memory (RAVLT), processing speed of information (SDMT), and fine motor coordination (GPT) were identical to the preoperative results. On the other hand, visuospatial memory (BVMT-R), visual attention (TMT A), and execution function (TMT B) declined more than one standard deviation compared to the preoperative data. Figure 6.1 presents the declined cognitive domains of Patient 1 with the corresponding brain regions. As discussed in Section 3.2, visuospatial memory is highly associated with right frontal lobes and temporal regions [53]. Declines in visual attention are correlated with parietal lobe atrophy, whereas execution functioning deficits are mainly corresponded to dysfunctions on left dorsomedial prefrontal cortex (dmPFC) [49, 62]. To further investigate brain activity within these brain regions, intraoperative fNIRS measurements are evaluated.

6.4.1.2 fNIRS analysis. As shown in Figure 6.2, CN 2-5 and 28-46 receive relatively low gain factors from 3-6, indicating that these channels receive strong hemodynamic signals. In contrast, most of CN 6-27, considered 'weak channels', are amplified with higher gain values from 7-8 because of noise arising from poor skin-optode contact. There are many possible reasons for weak channels, ranging from subject's characteristics to insufficient light coupling. Many studies have proposed that hair color and density significantly contribute to a great amount of light losses, decreasing quality of optical signals [82]. The NIRScap is often placed on the patient's head under a time constraint and restricted environment. For that reason, hair preparation before cap placement may not be performed thoroughly. Considering the hair characteristics of Patient 1, it is reasonable to assume that her hair may block

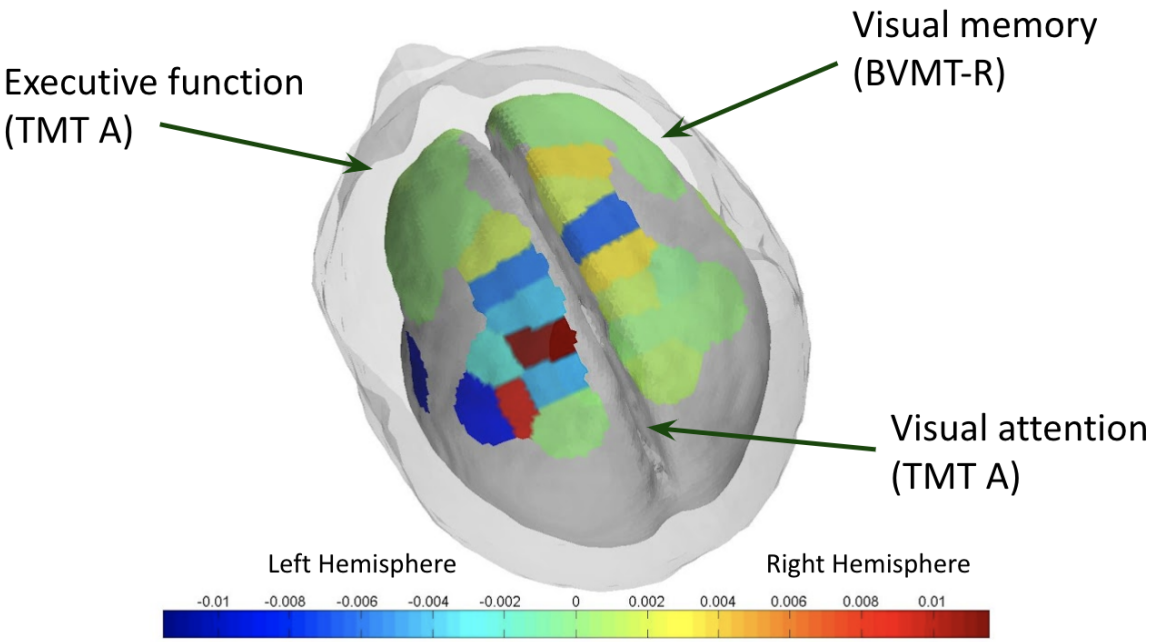

Figure 6.1. Brain regions associated with cognnitive declines of Patient 1. Visual memory: right frontal and temporal lobes; executive function: left dorsomedial prefrontal cortex (dmPFC); and visual attention: parietal lobes

optodes from reaching the scalp and thus interfere with light penetration. Another factor contributing to low signal quality is the location of channels. As presented in Figure 6.3, most of weak channels are located at the back of the head, where tight cables bending can easily occur due to subject's position during cardiac surgery. This potentially tilts the optodes and alters the traveling pathlength of light, reducing light transmission and thus resulting in weak signal detections. Although CN 6-27 appear as weak channels in detecting neuro-activation, there is still potential of hypoxia happening within the brain regions associated with these channels. Therefore, all channels must be taken into close consideration when examining for hypoxic events.

Results from one-sided t test suggested that within a bypass period, 20 of 46 channels were detected with oxygen desaturation in more than 5 of 1-minute interval. Of those 20 channels, CN 9, 11, 13, 17, and 46 are located in posterior parietal cortex. An average of detection times among CN 9, 11, 13 and 17 is fifteen, and each channel has at least one detection period of 2-minute interval. CN 46 yields 37 detection

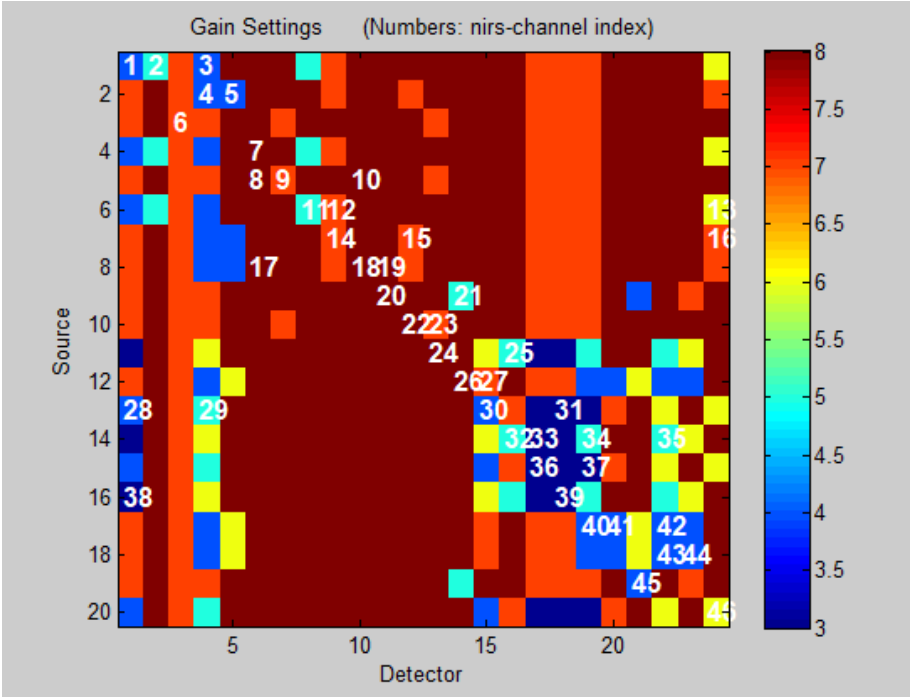

Figure 6.2. Gain map of Patient 1 indicates that most of channel 6-27 have relatively high gain values (7-8) while others have low gain values (2-5)

times and has seven periods of 2-minute interval. According to fNIRS results and neurocognitive findings, potential hypoxia in posterior parietal regions may decline visual attention performances. Since visual memory is highly associated with right frontal lobes, CN 41, 42, 43, and 44 are reviewed. An average of detection times among these channels are eleven. CN 41 and 44 have at least one detection period of 2-minute interval. Meanwhile, CN 42 and 43 are temporally correlated because both channels are detected with oxygen desaturation at the same time. In general, results from CN 41, 42, 43, and 44 are consistent with neurocognitive outcomes, indicating that lack of sufficient oxygen occurred in right frontal regions may lead to visual memory deficits. Lastly, Patient 1 also has severe declines in executive function, which is controlled by left dmPFC. Within this brain region, CN 27, 29, and 30 have relatively high detection times. CN 27 and 30 are detected with 19 times of oxygen desaturation and have at least three periods of 2-minute interval. Among the 20 channels, CN 29 provides the highest detection of oxygen desaturation, at 45

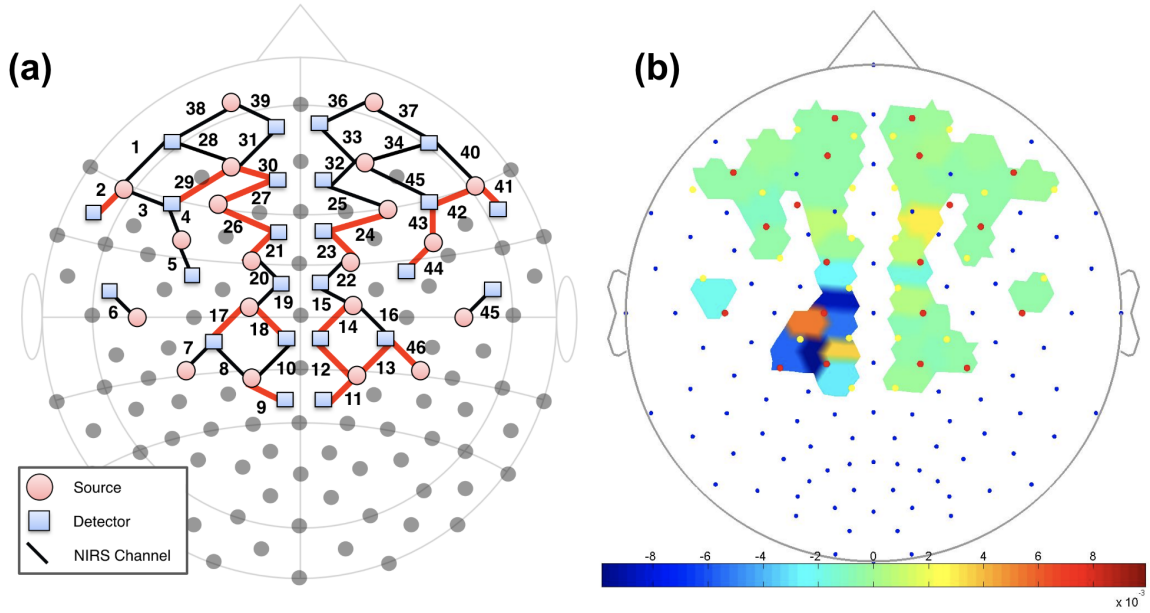

Figure 6.3. (a) Locations of 46 channels with respect to the scalp, and red lines indicate channels with more than 5 detection times of potential hypoxia, (b) a heatmap of relative changes in milliMolar (mM) in oxygenated hemoglobin [HbO_2] of Patient 1

times; the channel has eight periods of 2-minute interval, one of 4-minute interval, and one of 8-minute interval. Even though the study provides promising results, it is important to notice that the current technique is only capable of detecting the number of oxygen desaturation. Future research is needed to eliminate noise in weak channels and validate a correlation between the detection times and the actual hypoxic events.

6.4.2 Case 2

Patient 2 is a 65 year old Caucasian male who underwent CABG. He had short, thick hair with brown color. He had 9 years of education and no history of neurologic conditions or stroke.

6.4.2.1 Neurocognitive analysis. At baseline, both verbal memory (RAVLT) and visual memory (BVMT) were significantly below average compared to normative data. His performances of visual attention (TMT A), executive function (TMT B), processing speed of information (SDMT), and fine motor skills (SDMT) were

mildly below average relative to matched age norms. About 20 days after surgery, his verbal memory (RAVLT) declined about one standard deviation compared to preoperative data, while his visual memory (BVMT) improved approximately two standard deviations. There was a slight improvement in visual attention (TMT A) and executive function (TMT B). On the other hand, performances of information processing speed (SDMT) and fine motor coordination (GPT) were slightly declined. Overall, significant declines in verbal memory (RAVLT) of Patient 2 suggest that there is potential damage in multiple regions within left hemisphere, including prefrontal cortex, frontal, and parietal lobes (Figure 6.4) [49]. To examine these brain regions, intraoperative fNIRS measurements are reviewed.

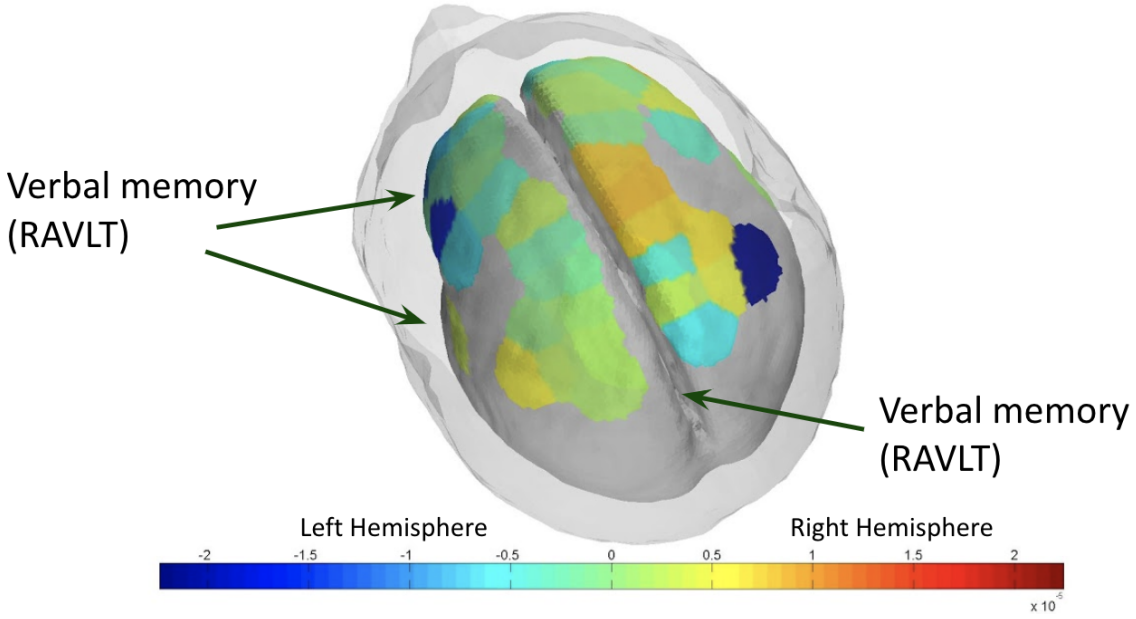

Figure 6.4. Brain regions associated with cognnitive declines of Patient 2. Verbal memory: left hemisphere of the brain, including prefrontal cortex, frontal, and parietal lobes

6.4.2.2 fNIRS analysis. Results from the signal quality check showed that all 46 channels provided a good amount of hemodynamic signal with low amplification levels, ranging from 2-5 (Figure 6.5). Ten of 46 channels are detected with more than 5 times of oxygen desaturation. Three of the 10 channels, consisting of CN 7, 14, and

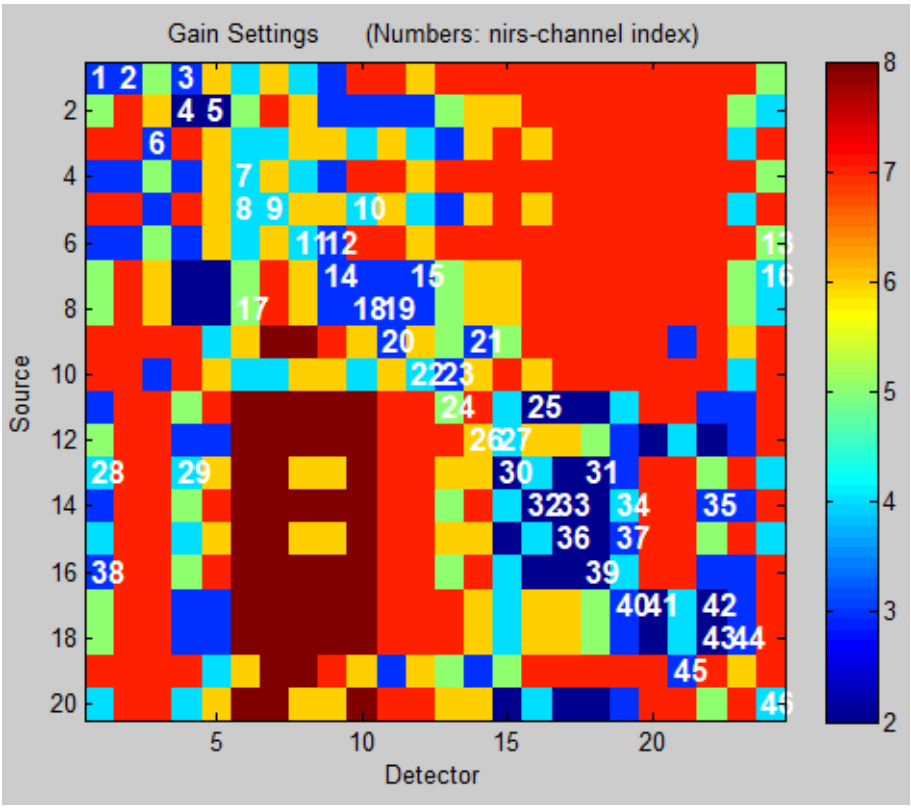

Figure 6.5. Gain map of Patient 2 shows that all 46 channels have low amplification, ranging from 2-5

16, do not exhibit consecutive sequence of detection. Compared to Patient 1, Patient 2 has lower number of channels detected with oxygen desaturation; however, the time interval of consecutive detections is slightly longer, at 3 minutes. Longer duration of oxygen desaturation may result in greater cognitive deficits [76].

The location of fNIRS channels respective to the scalp are illustrated in Figure 6.6. CN 28 and 9 are located at prefrontal cortex and parietal lobes, respectively; both channels have highest number of oxygen desaturation, at 10 times and two detection periods: one of 2-minute interval and one of 3-minute interval. In addition, CN 10, which correlates with measurements at parietal lobes and CN 21, which corresponds to data obtained from frontal lobes have an average detection of 8 times and one period of 3-minute interval. As a result, the high number of oxygen desaturation found among CN 9, 10, 21, and 28 suggests that potential hypoxia may

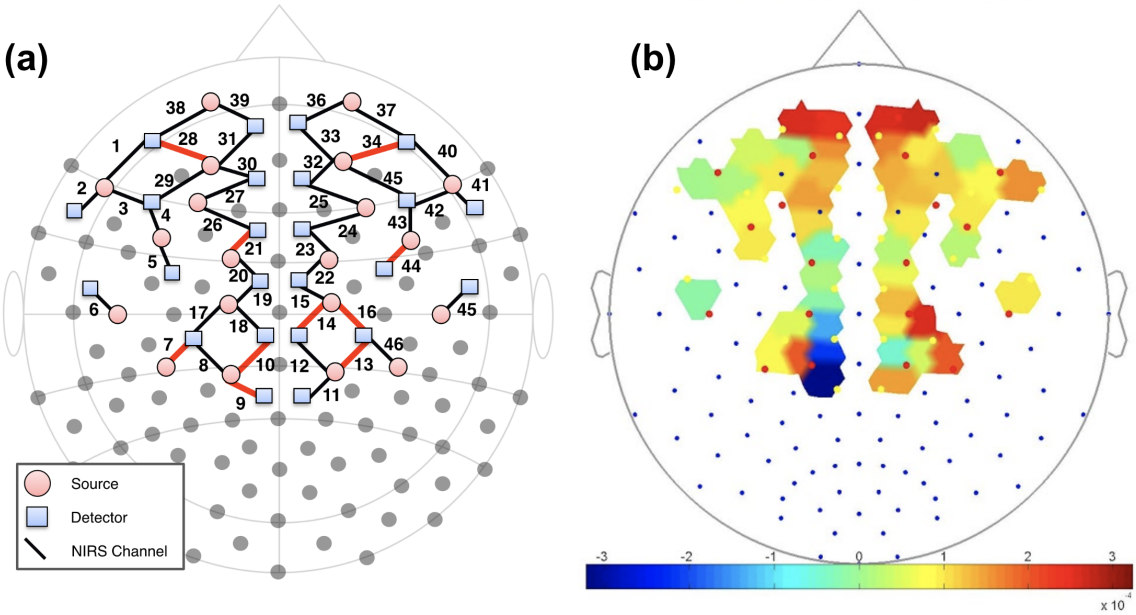

Figure 6.6. (a) Locations of 46 channels with respect to the scalp, and red lines indicate channels with more than 5 detection times of potential hypoxia, (b) a heatmap of relative changes in milliMolar (mM) in oxygenated hemoglobin $[HbO_2]$ of Patient 2

cause damage in the prefrontal cortex and the parietal lobes and hence result in verbal memory impairments. Other channels such as CN 34 and CN 44 are also detected with 9 times of oxygen desaturation and have at least one period of 2-minute interval. Although declines in neurocognitive performances of Patient 2 do not indicate impairments in the right frontal lobes, hypoxia may occur within these regions. The research requires a more in-depth study to investigate underlying causes of these detections.

CHAPTER SEVEN

Conclusion

The first section of this chapter provides a summary of the study in Section 7.1. The following sections discuss research limitations in Section 7.2 and suggest directions for future work in Section 7.3.

7.1 Synopsis of Research

The aim of the study was to demonstrate the utility of the high-density fNIRS technique in intraoperative monitoring of cerebral oxygenation at extended brain areas, including prefrontal cortex, frontal lobes, and posterior parietal cortex. The study comprised fNIRS measurements, which were recorded during cardiac surgery and neurocognitive assessments, which were given at three time points: prior to surgery, hospital discharge, and the first follow-up clinical visit.

Considering various experimental constraints, the protocol of the study was constantly developed to improve data quality and ensure safety. The fNIRS montage was designed with an optimal optode arrangement to monitor the regions of interest. The proper technique of the cap placement was established to maximize skin-optode contact, allowing good data acquisition. Moreover, the layout of the intraoperative equipment setup was taken in great consideration to enhance signal quality, provide patient's comfort, and prevent instrument damage. During an intraoperative fNIRS monitoring, recording motion artifacts and surgical events was essential in determining baseline and bypass duration for data analysis. Cleaning procedures for the NIRScap and imaging devices were developed to maintain high standards of hygiene.

In this study, a comprehensive test battery was utilized to assess the following cognitive domains: verbal memory, visual memory, visual attention, executive function, processing speed of information, and fine motor coordination. The baseline

and postoperative assessments of 12 patients were reviewed. At a group-level, there was a significant decline in verbal memory after cardiac surgery. In contrast, the statistically significant results revealed that there was no difference between pre- and postoperative performances among other cognitive domains. At a single-subject level, two case studies were discussed in great detail. Cognitive performances of pre- and postoperative assessments of two patients were evaluated to identify their cognitive impairments after cardiac surgery. fNIRS measurements were processed using nirsLAB, and the data was further analyzed using the developed processing code in Matlab. In both case studies, the results from one-sided t-tests indicated a high number of oxygen desaturation within brain regions associated with neurocognitive impairments. The study demonstrated that the current fNIRS technique was capable of detecting potential hypoxia along with an approximate duration of the hypoxic events.

Previously, Mohandas and his colleagues performed the study on 100 patients undergoing cardiac surgery with CPB and utilized the NIRS-based cerebral oximiter as the monitoring modality [83]. The study reported that patients who were detected with oxygen desaturation at greater brain regions suffered significant neurocognitive declines [83]. Similarly, Colak and his group recruited 200 CABG patients and employed INVOS device to monitor cerebral oxygenation intraoperatively [84]. The findings of Colak's study reported that patients with intraoperative cerebral oxygenation monitoring resulted in better cognitive outcomes subsequent to cardiac surgery [84]. Furthermore, prolonged oxygen desaturation was found as an important factor in determining cognitive declines [84]. Despite the relatively small sample size, the current study produced promising results in support of previous research, which suggested fNIRS measurements of cerebral oxygenation as an indicator of potential hypoxia [27, 83, 84]. The current study has a clear potential for prospective cohort study at a larger scale. With a more well-defined protocol, the methodology of the

study can be used to avoid bias, maintain consistency, and allow fair assessments across study populations.

7.2 Research Limitations

Even though many studies have evidenced positive outcomes of intraoperative fNIRS monitoring in detecting early oxygen desaturation, there is a further need to validate the reliability of fNIRS data, as well as verifying the use of fNIRS technique in indicating POCD candidates. To further improve the quality of the research, several limitations of the current study, ranging from data collection to data analysis need to be addressed.

Ideally, the baseline is established during a resting state in which prior to the recording session, the subjects comfortably lay down or sit still in a dark, quiet room while relaxing their body and minimizing movement [85]. These environmental conditions reduce external distractions and achieve reliable baseline measurements. However, this traditional approach is not feasible for studies happening in a more constrained setting, like an operating room. In the study, the baseline was acquired after induction of anesthesia and recorded approximately 5-10 minutes before the first incision on the patient's chest. Anesthetic agents, however, might greatly alter the cerebral blood flow (CBF) in brain regions and hence lead to significant changes in hemodynamic and cerebral metabolism [86]. In addition to the effects of anesthesia, unwanted movements introduced motion artifacts to fNIRS data. Many studies have reported that measuring preoperative values at any time point before induction of anesthesia provides more accurate estimates of the baseline. This eliminates the effects of anesthesia during the baseline recording [28, 72].

A major source of noise in fNIRS measurements is caused by systemic interferences arising from physiological signals such as cardiac output, respiratory pulses, and blood pressure. To date, there is no standardized method to completely reduce

this noise from the data. In an attempt to address this drawback of fNIRS technique, numerous studies have proposed the use of independent principal component analysis (ICA) to decompose obtained signals into distinct components and thus allow detection of artifacts [87, 88]. Indeed, ICA is a popular technique for feature extractions in the field of EEG research; however, the applications of ICA require a strong assumption about temporal independence and spatial stationarity of each source [89, 90]. Another approach of systemic interference reduction is to utilize multidistance channels in the imaging modality. Short distance channels with a SD separation of less than 1 cm are efficient in measuring physiological signals in the superficial layers since NIR light can only reach the outer superficial layers at this SD seperation [91]. Therefore, short distance channels are referred to as references for systemic noises and therefore can be used as regressors to identify physiological interferences present in longer SD measurements, often measured at more than 3 cm [92]. These techniques can be applied in future study to provide more reliable fNIRS measurements.

7.3 Future Directions

The next steps of the current study are to standardize the fNIRS imaging procedure and improve fNIRS data and neurocognitive assessments. Proper hair preparation is needed to maximize skin-optode contact, resulting in high fNIRS signal quality. An addition of optical gel will also improve light connectivity. By implementing reference channels and developing a standard function for physiological interference reduction, fNIRS measurements become reliable and hence provide accurate indicators of oxygen desaturation. In addition, Barker's study has suggested that comparing to the standard deviation (SD) method, the reliable change index (RCI) is more effective in accounting for practice effects [81]. Therefore, reliable changes of neurocognitive functions will be assessed using the RCI.

The main focus of future work is to validate the intraoperative fNIRS monitoring technique in a larger diverse population. With an adequate amount of high-quality data, a learning algorithm will be developed to train neural networks which detect oxygen imbalance and provide reasonable warnings of potential hypoxia and other adverse events. The neural networks will eventually evolve into an automated system that predicts adverse events and enables performance of early interventions during cardiac surgery.

APPENDICES

APPENDIX A

A Summary of Neurocognitive Measures

The test battery used in the study consists of six following tests.

Rey Auditory Verbal Learning Test (RAVLT): The test consists of 5 learning trials, 1 interfering trial, 1 delayed trial, and 1 recognition trial. A 15 noun-word list (list A) was read to the participant at the rate of one per second. The participant is requested to recall as many words as possible. This procedure is repeated 5 times. After 5 learning trials of list A, a second list of 15 other nouns (list B) was read to the participant, who is requested to recall the words. Immediately after the recall of list B, the participant is asked to recall list A. After a 20-min delay, the participant is again asked to recall list A. For recognitional trial, the participant receives a list of words and is asked to indicate which words were from the first list. The performance is measured based on the number of correct responses [48].

Brief Visuospatial Memory Test Revised (BVMT-R): The test includes 3 learning trails, 1 delayed trial, and 1 recogcognition trial. The participant is asked to look at six geometric figures arranged in 2x3 array for 10 seconds. After the figures taken away, the participant immediately draws the figures in their accurate forms and exact locations. The procedure is repeated for 3 learning trial. After a 25-min distraction-filled delay, the participant is again asked to draw the figures from memory. Following a delayed trial, 12 figures are shown to the participant one at a time, and the participant is asked to indicate whether each figure was in the stimuli set. The overall performance is based on the number of figures that are correctly reproduced and recognized [53].

Symbol Digit Modalities Test (SDMT): The participant is presented a reference key of symbol-number combinations at the top of the page. Within 90 seconds, the

participant is requested to pair symbols with corresponding numbers. The performance is measured based on a number of corrected matching pairs [57].

Trail-Making Test (TMT A&B): The test consists of 2 parts: A and B. In part A, the participant is asked to draw a continuous line connecting circled numbers in a numerical order, as quickly as possible (ie. 1-2-3). In part B, the participant is asked to draw a continuous line alternating between numbers and letters in a numerical and alphabetic order, as quickly as possible (ie. 1-A-2-B-3-C). The performance is measured based on the completion time of each task [61].

Grooved Pegboard Test (GPT): The test includes 2 trials: one with the dominant hand and one with the non dominant hand. The test consists of a pegboard that has 25 holes with randomly positioned slots and pegs with a square and a rounded side. Using only one hand at a time, the participant has to rotate the pegs to fit and insert into the holes. The performance is measured based the completion time of each trial [64].

Wechsler Test of Adult Reading (WTAR): A list of 50 words with irregular pronunciations is shown to the participant who is then asked to read out loud words in listed order. The performance is measured based on the number of correct pronounced words [67].

APPENDIX B

Equipment Cleaning

B.1 Imaging Devices

(1) Clean optodes with Soft-zellin or Webcol wipes
    - Never clean optodes with premoistened clean-wipes or Sani-cloth
(2) Clean cables and wires with Fisherbrand premoistened clean-wipes (Alcohol/DI water)
(3) Clean a strain-relief arm and workstation with Sani-cloth
(4) Remove dried blood stains on cables and wires:
    - Spray a cotton ball with cold water
    - Place the damp cotton ball directly on the stained spot for 5 mins
        * Prevent water from dripping into electrical hardware areas
    - Rub the cables or wires gently with the damp cotton ball
    - Use damp cotton swabs to remove small blood stains or residuals

B.2 NIRScap

Note: This procedure can be used to clean an overcap, NIRScaps, and cable trees. Optode holders and labels can be remained on the cap for washing.

B.2.1 Routine Cleaning

(1) Wear protective clothing: gloves
(2) Remove all optodes
(3) Flip cap inside out
(4) Use 2-3 pumps of PVP Scrub Solution
(5) Leave cap soaked in the solution for 30 seconds
(6) Place one hand inside cap

(7) Use other hand to gently wash the outside of cap in a circular motion

(8) Rinse cap with tap water twice to remove residuals

(9) Repeat step 4-8 with shampoo

(10) Remove excess water with paper towels

(11) Place cap between a clean towel

(12) Store cap in a dry area and avoid direct sunlight

B.2.2 Deep Disinfection

(1) Wear suitable protective clothing: gloves

(2) Produce the disinfection solution by diluting with water in the designated bucket. Mix 40 ml of Sekusept with 960 ml of water.

- Solution is to prepared fresh daily and reusable for all participants within one day

(3) Soak cap in the solution for 15 minutes

(4) Rinse cap with tap water

BIBLIOGRAPHY

[1] A. Pisano, N. Galdieri, T. P. Iovino, M. Angelone, and A. Corcione. Direct comparison between cerebral oximetry by invostm and equanoxtm during cardiac surgery: a pilot study. *Heart, Lung and Vessels*, 6(3):197–203, 2014.

[2] Medmovies.com. Coronary artery bypass graft(CABG).

[3] H. Bishop and B. Middleton. Cardiopulmonary bypass. *Surgery (Oxford)*, 36(2):63–67, Feb 2018.

[4] Dutch Renaissance Press. Brain diagram.

[5] M. Ferrari and V. Quaresima. A brief review on the history of human functional near-infrared spectroscopy (fnirs) development and fields of application. *NeuroImage*, 63(2):921–935, Nov 2012.

[6] A. Pellicer and M. C. Bravo. Near-infrared spectroscopy: A methodology-focused review. *Seminars in Fetal and Neonatal Medicine*, 16(1):42–49, Feb. 2011.

[7] N. Naseer and K.S. Hong. fnirs-based brain-computer interfaces: a review. *Frontiers in Human Neuroscience*, 9, Jan 2015.

[8] F. Scholkmann et al. A review on continuous wave functional near-infrared spectroscopy and imaging instrumentation and methodology. *NeuroImage*, 85:6–27, Jan. 2014.

[9] NIRx Medical Technologies LLC. *NIRScout User Guide*.

[10] X. Yong and H. Graber ad R. Barbour. *nirsLAB User Manual*. SUNY Downstate Medical Center, NIRx Medical Technologies LLC.

[11] D. L. McDonagh, M. Berger, J. P. Mathew, Carmelo C. Graffagnino, C. A. Milano, and M. F. Newman. Neurological complications of cardiac surgery. *The Lancet Neurology*, 13(5):490–502, May 2014.

[12] M. Berger et al. Postoperative cognitive dysfunction. *Anesthesiology Clinics*, 33(3):517–550, Sep. 2015.

[13] G. A. Mashour, D. T. Woodrum, and M. S. Avidan. Neurological complications of surgery and anaesthesia. *BJA: British Journal of Anaesthesia*, 114(2):194–203, Sep. 2014.

[14] J. Steinmetz, K. B. Christensen, T. Lund, N. Lohse, and L. S. Rasmussen. Long-term Consequences of Postoperative Cognitive Dysfunction. *Anesthesiology: The Journal of the American Society of Anesthesiologists*, 110(3):548–555, Mar. 2009.

[15] A. E. Harten, T. W. L. Scheeren, and A. R. Absalom. A review of postoperative cognitive dysfunction and neuroinflammation associated with cardiac surgery and anaesthesia. *Anaesthesia*, 67(3):280–293, Feb. 2012.

[16] J. Beca and D. Sidebotham. Chapter 37 - neurologic dysfunction. In M. Gillham D. Sidebotham, A. Mckee and J. H. Levy, editors, *Cardiothoracic Critical Care*, page 558. Butterworth-Heinemann, Jan. 2007.

[17] G. Vretzakis et al. Cerebral oximetry in cardiac anesthesia. *Journal of Thoracic Disease*, 6 Suppl 1:S60–S69, Mar. 2014.

[18] F. Guarracino, R. Baldassarri, and P. Zanatta. Current status of neuromonitoring in cardiac surgery. *Current Anesthesiology Reports*, 7:1–6, July 2017.

[19] T. J. Kimberley and S. M Lewis. Understanding Neuroimaging. *Physical Therapy*, 87(6):670–683, June 2007.

[20] S. Baillet, J. C. Mosher, and R. M. Leahy. Electromagnetic brain mapping. *IEEE Signal Processing Magazine*, 18(6):14–30, Nov 2001.

[21] R. P. Lystad and H. Pollard. Functional neuroimaging: a brief overview and feasibility for use in chiropractic research. *The Journal of the Canadian Chiropractic Association*, 53(1):59–72, March 2009.

[22] D. A. Boas, C. E. Elwell, M. Ferrari, and G. Taga. Twenty years of functional near-infrared spectroscopy: introduction for the special issue. *NeuroImage*, 85:1–5, Jan. 2014.

[23] T. J. Huppert, M. A. Franceschini, and D. Boas. Chapter 14 - noninvasive imaging of cerebral activation with diffuse optical tomography. In R.D. Frostig, editor, *In Vivo Optical Imaging of Brain Function*, page 280. Taylor & Francis, May 2009.

[24] V. Quaresima, S. Bisconti, and M. Ferrari. A brief review on the use of functional near-infrared spectroscopy (fnirs) for language imaging studies in human newborns and adults. *Brain and Language*, 121(2):79–89, 2012.

[25] F. Zheng, R. Sheinberg, M. S. Yee, M. Ono, Y. Zheng, and C. W. Hogue. Cerebral near-infrared spectroscopy (nirs) monitoring and neurologic outcomes in adult cardiac surgery patients and neurologic outcomes: A systematic review. *Anesthesia and analgesia*, 116(3), Mar. 2013.

[26] S. N. Davie and H.P. Grocott. Impact of extracranial contamination on regional cerebral oxygen saturationa comparison of three cerebral oximetry technologies. *Anesthesiology: The Journal of the American Society of Anesthesiologists*, 116(4):834–840, Apr. 2012.

[27] J. M. Murkin and M. Arango. Near-infrared spectroscopy as an index of brain and tissue oxygenation. *BJA: British Journal of Anaesthesia*, 103(Supplement 1):i3–i13, Dec. 2009.

[28] M. J. Chan, N. J. Glassford T. Chung, and R. Bellomo. Near-infrared spectroscopy in adult cardiac surgery patients: A systematic review and meta-analysis. *Journal of Cardiothoracic and Vascular Anesthesia*, 31(4):1155–1165, Aug. 2017.

[29] F. H Epstein and C.C.W Hsia. Respiratory function of hemoglobin. *The New England journal of medicine*, 338(4):239–248, Jan 22 1998. Copyright - Copyright 1998 Massachusetts Medical Society. All rights reserved; Last updated - 2017-10-31; CODEN - NEJMAG.

[30] R. M. Pearse and A. Rhodes. *Mixed and Central Venous Oxygen Saturation*, volume 2005, pages 592–602. Springer-Verlag, 2005.

[31] J. Holm, E. Hkanson, F. Vnky, and R. Svedjeholm. Mixed venous oxygen saturation predicts short- and long-term outcome after coronary artery bypass grafting surgery: a retrospective cohort analysis. *BJA: British Journal of Anaesthesia*, 107(3):344–350, Sep 2011.

[32] X. H. Krauss P. D., Verdouw, P. G. Hughenholtz, and J. Nauta. On-line monitoring of mixed venous oxygen saturation after cardiothoracic surgery. *Thorax*, 30(6):636–643, 1975.

[33] M. Diodato and E.G. Chedrawy. Coronary artery bypass graft surgery: The past, present, and future of myocardial revascularisation. *Surgery Research and Practice*, 2014.

[34] H. Saad and M. Aladawy. Temperature management in cardiac surgery. *Global Cardiology Science & Practice*, 2013(1):44–62, Nov 2013.

[35] D. Machin and C. Allsager. Principles of cardiopulmonary bypass. *Continuing Education in Anaesthesia Critical Care & Pain*, 6(5):176–181, Oct 2006.

[36] M. Sarkar and V. Prabhu. Basics of cardiopulmonary bypass. *Indian Journal of Anaesthesia*, 61(9):760–767, Sep 2017.

[37] L. Vera-Portocarrero. *Brain Facts*. Gray matter. Chelsea House, 2007.

[38] D. T. Stuss and R.T. Knight. *Principles of Frontal Lobe Function*. OUP USA, 2013.

[39] D. Attwell, A. M. Buchan, S. Charpak, M. Lauritzen, B. A. MacVicar, and E. A. Newman. Glial and neuronal control of brain blood flow. *Nature*, 468(7321):232–243, Nov. 2010.

[40] H. Y. Kim, K. Seo, H. J. Jeon, U. Lee, and H. Lee. Application of functional near-infrared spectroscopy to the study of brain function in humans and animal models. *Molecules and Cells*, 40(8):523–532, Aug. 2017.

[41] S. L. Jacques. Optical properties of biological tissues: a review. *Physics in Medicine & Biology*, 58(11):R37, 2013.

[42] M. Izzetoglu et al. Functional near-infrared neuroimaging. *IEEE Transactions on Neural Systems and Rehabilitation Engineering*, 13(2):153–159, Jun 2005.

[43] T. J. Huppert, S. G. Diamond, M. A. Franceschini, and D. A. Boas. Homer: a review of time-series analysis methods for near-infrared spectroscopy of the brain. *Applied optics*, 48(10):D280–D298, Apr. 2009.

[44] G. E. Strangman, Z. Li, and Q. Zhang. Depth sensitivity and source-detector separations for near infrared spectroscopy based on the colin27 brain template. *PLOS ONE*, 8(8):1–13, Aug. 2013.

[45] G. Strangman, D. A. Boas, and Jeffrey P J. P. Sutton. Non-invasive neuroimaging using near-infrared light. *Biological Psychiatry*, 52(7):679–693, Oct 2002.

[46] J. M. Murkin, S. P. Newman, D. A. Stump, and J. A. Blumenthal. Statement of consensus on assessment of neurobehavioral outcomes after cardiac surgery. *The Annals of Thoracic Surgery*, 59(5):1289–1295, May 1995.

[47] I. Rundshagen. Postoperative cognitive dysfunction. *Deutsches rzteblatt International*, 111(8):119–125, Feb 2014.

[48] A. C. Ferreira and I. O. Campagna. The rey auditory verbal learning test: Normative data developed for the venezuelan population. *Archives of Clinical Neuropsychology*, 29(2):206–215, Mar 2014.

[49] S. E. MacPherson et al. Processing speed and the relationship between trail making test-b performance, cortical thinning and white matter microstructure in older adults. *Cortex; a Journal Devoted to the Study of the Nervous System and Behavior*, 95:92–103, Oct 2017.

[50] M. L. F. Balthazar, C. L. Yasuda, F. Cendes, and B. P. Damasceno. Learning, retrieval, and recognition are compromised in amci and mild ad: Are distinct episodic memory processes mediated by the same anatomical structures? *Journal of the International Neuropsychological Society*, 16(01):205, Jan 2010.

[51] D. W. Loring et al. Differential neuropsychological test sensitivity to left temporal lobe epilepsy. *Journal of the International Neuropsychological Society*, 14(03):394–400, May 2008.

[52] E. Moradi, I. Hallikainen, T. Hnninen, and J. Tohka. Reys auditory verbal learning test scores can be predicted from whole brain mri in alzheimers disease. *NeuroImage: Clinical*, 13:415–427, Dec 2016.

[53] E. Graziol, A. E. Yeh, R.HB. Benedict, J. Parrish, and B. Weinstock-Guttman. Cognitive dysfunction in ms: bridging the gap between neurocognitive deficits, neuropsychological batteries and mri. *Future Neurology*, 3(1):49–59, 2008.

[54] J. W. Tam and M. Schmitter-Edgecombe. The role of processing speed in the brief visuospatial memory test - revised. *The Clinical neuropsychologist*, 27(6):962–972, Aug. 2013.

[55] R. H. B. Benedict, D. Schretlen, L. Groninger, M. Dobraski, and B. Shpritz. Revision of the brief visuospatial memory test: Studies of normal performance, reliability, and validity. *Psychological Assessment*, 8(2):145–153, Jun 1996.

[56] E. C. McIntosh et al. Does medial temporal lobe thickness mediate the association between risk factor burden and memory performance in middle-aged or older adults with metabolic syndrome? *Neuroscience Letters*, 636:225–232, Jan 2017.

[57] K. M. Kiely, P. Butterworth, N. Watson, and M. Wooden. The symbol digit modalities test: Normative data from a large nationally representative sample of australians. *Archives of Clinical Neuropsychology*, 29(8):767–775, Dec 2014.

[58] C. Forn et al. A symbol digit modalities test version suitable for functional mri studies. *Neuroscience Letters*, 456(1):11–14, May 2009.

[59] C. Forn et al. A comparison of brain activation patterns during covert and overt paced auditory serial addition test tasks. *Human brain mapping*, 29(6):644–650, June 2008.

[60] B. Brochet et al. Should SDMT substitute for PASAT in MSFC? a 5-year longitudinal study. *Multiple Sclerosis Journal*, 14(9):1242–1249, Nov 2008.

[61] E. L. Misdraji and C.S. Gass. The trail making test and its neurobehavioral components. *Journal of Clinical and Experimental Neuropsychology*, 32(2):159–163, Feb 2010.

[62] N. Miskin et al. Prefrontal lobe structural integrity and trail making test, part b: converging findings from surface-based cortical thickness and voxel-based lesion symptom analyses. *Brain Imaging and Behavior*, 10(3):675–685, 2016.

[63] S. Wagner, I. Helmreich, N. Dahmen, K. Lieb, and A. Tadi. Reliability of three alternate forms of the trail making tests a and b. *Archives of Clinical Neuropsychology*, 26(4):314–321, Jun 2011.

[64] L. Ashendorfand J. L. Vanderslice-Barr and R. J. McCaffrey. Motor tests and cognition in healthy older adults. *Applied Neuropsychology*, 16(3):171–176, Aug 2009.

[65] O. Bezdicek et al. Grooved pegboard predicates more of cognitive than motor involvement in parkinsons disease. *Assessment*, 21(6):723–730, Dec 2014.

[66] T. K. Rosengart el at. Stable cognition after coronary artery bypass grafting: Comparisons with percutaneous intervention and normal controls. *The Annals of Thoracic Surgery*, 82(2):597–607, Aug 2006.

[67] K. A. Whitney, P. H. Shepard, J. Mariner, B. Mossbarger, and S. M. Herman. Validity of the wechsler test of adult reading (wtar): Effort considered in a clinical sample of u.s. military veterans. *Applied Neuropsychology*, 17(3):196–204, Sep 2010.

[68] R. E. A. Green, B. Melo, B. Christensen, Le-Anh Ngo, G. Monette, and C. Bradbury. Measuring premorbid iq in traumatic brain injury: An examination of the validity of the wechsler test of adult reading (wtar). *Journal of Clinical & Experimental Neuropsychology*, 30(2):163–172, Feb 2008.

[69] K. A. Steward, T. A. Novack, R. Kennedy, M. Crowe, D. C. Marson, and K. L. Triebel. The wechsler test of adult reading as a measure of premorbid intelligence following traumatic brain injury. *Archives of Clinical Neuropsychology*, 32(1):98–103, Feb 2017.

[70] A. Kassab and M. Sawan. The nirs cap: Key part of emerging wearable brain-device interfaces. *Developments in Near-Infrared Spectroscopy*, Mar. 2017.

[71] X. Yong and H. Graber ad R. Barbour. *NIRstar User Manual*. NIRx Medical Technologies LLC.

[72] W. Tosh and M. Patteril. Cerebral oximetry. *BJA Education*, 16(12):417–421, Dec 2016.

[73] Donders Institute. *Disinfection and cleaning procedure EEG equipment*.

[74] K. L. M. Koenraadt, E. G. Roelofsen, J. Duysens, and N. L. W. Keijsers. Cortical control of normal gait and precision stepping: An fnirs study. *NeuroImage*, 85:415–422, Jan 2014.

[75] S. S. Razaand F. Ullah, N. Chandni, and E. B. Savage. Cerebral oximetry use for cardiac surgery. *Journal of Ayub Medical College, Abbottabad: JAMC*, 29(2):335–339, Jun 2017.

[76] M. L. Turetz and R. G. Crystal. *Mechanisms and Consequences of Central Nervous System Hypoxia*. Academic Press, Jan 2007.

[77] S. Meja-Arango, R. Wong, and A. Michaels-Obregn. Normative and standardized data for cognitive measures in the mexican health and aging study. *Salud publica de Mexico*, 57(0 1):S90–S96, 2015.

[78] J. Vardy, S. Rourke, and I. F Tannock. Evaluation of cognitive function associated with chemotherapy: A review of published studies and recommendations for future research. *Journal of Clinical Oncology*, 25(17):2455–2463, Jun 2007.

[79] E. Symes, P. Maruff, A. Ajani, and J. Currie. Issues associated with the identification of cognitive change following coronary artery bypass grafting. *Australian & New Zealand Journal of Psychiatry*, 34(5):770–784, Oct 2000.

[80] K. S. Funder, J. Steinmetz, and L. S. Rasmussen. Methodological issues of postoperative cognitive dysfunction research. *Seminars in Cardiothoracic and Vascular Anesthesia*, 14(2):119–122, Jun 2010.

[81] S. L. Barker-Collo, L. Suzanne, and S. C Purdy. Determining the presence of reliable change over time in multiple sclerosis. *International Journal of MS Care*, 15(4):170–178, 2013.

[82] B. Khan el at. Improving optical contact for functional nearinfrared brain spectroscopy and imaging with brush optodes. *Biomedical Optics Express*, 3(5):878–898, Apr 2012.

[83] B. S Mohandas, A. M. Jagadeesh, and S. B. Vikram. Impact of monitoring cerebral oxygen saturation on the outcome of patients undergoing open heart surgery. *Annals of Cardiac Anaesthesia*, 16(2):102, Apr 2013.

[84] Z. Colak el at. Influence of intraoperative cerebral oximetry monitoring on neurocognitive function after coronary artery bypass surgery: a randomized, prospective study. *European Journal of Cardio-Thoracic Surgery*, 47(3):447–454, Mar 2015.

[85] Y. Zhang et al. Multiregional functional near-infrared spectroscopy reveals globally symmetrical and frequency-specific patterns of superficial interference. *Biomedical Optics Express*, 6(8):2786–2802, Jul 2015.

[86] L. Ciobanu, O. Reynaud, L. Uhrig, B. Jarraya, and D. Le Bihan. Effects of anesthetic agents on brain blood oxygenation level revealed with ultra-high field mri. *PLoS ONE*, 7(3), Mar 2012.

[87] Y. Jiao, Z. Zhou, H. Yang, Z. Ruan, H.Gong, and Z.Lu. Independent component analysis of event-related functional near-infrared spectroscopy (fnirs). *2008 International Conference on BioMedical Engineering and Informatics*, 2:440–444, 2008.

[88] Y. Zhang, X. Liu, C. Yang, K. Wang, J. Sun, and P. Rolfe. A new approach to separate haemodynamic signals for brain-computer interface using independent component analysis and least squares. *Journal of Spectroscopy*, 2013:1–9, 2013.

[89] P. LeVan, E. Urrestarazu, and J. Gotman. A system for automatic artifact removal in ictal scalp eeg based on independent component analysis and bayesian classification. *Clinical Neurophysiology*, 117(4):912–927, Apr 2006.

[90] A. Aarabi and T. J. Huppert. Characterization of the relative contributions from systemic physiological noise to whole-brain resting-state functional near-infrared spectroscopy data using single-channel independent component analysis. *Neurophotonics*, 3(2), Apr 2016.

[91] S. Brigadoi, Sabrina, and R. J. Cooper. How short is short? Optimum sourcedetector distance for short-separation channels in functional near-infrared spectroscopy. *Neurophotonics*, 2(2), Apr 2015.

[92] L. Gagnon, R. J. Cooper, M. A. Ycel, K. L. Perdue, D. N. Greve, and D. A. Boas. Short separation channel location impacts the performance of short channel regression in nirs. *Neuroimage*, 59(3):2518–2528, Feb 2012.